RESEARCH ARTICLE

A p75 neurotrophin receptor-sparing nerve growth factor protects retinal ganglion cells from neurodegeneration by targeting microglia

Laura Latini[1] | Daniel Souza Monteiro De Araujo[2] | Rosario Amato[3] |
Alessio Canovai[3] | Lucia Buccarello[1] | Francesco De Logu[2] | Elena Novelli[4] |
Anastasiia Vlasiuk[5,6] | Francesca Malerba[1] | Ivan Arisi[1] | Rita Florio[1] |
Hiroki Asari[5] | Simona Capsoni[7,8] | Enrica Strettoi[4] | Gino Villetti[9] |
Bruno Pietro Imbimbo[9] | Massimo Dal Monte[3] | Romina Nassini[2] |
Pierangelo Geppetti[2] | Silvia Marinelli[1] | Antonino Cattaneo[1,7]

[1]European Brain Research Institute-Fondazione Rita Levi-Montalcini, Rome, Italy

[2]Department of Health Sciences, Clinical Pharmacology and Oncology Section, University of Florence, Florence, Italy

[3]Department of Biology, University of Pisa, Pisa, Italy

[4]Institute of Neuroscience, Italian National Research Council–CNR, Pisa, Italy

[5]Faculty of Biosciences, Collaboration for Joint PhD Degree Between EMBL and Heidelberg University, Heidelberg, Germany

[6]Epigenetics and Neurobiology Unit, EMBL Rome, European Molecular Biology Laboratory, Rome, Italy

[7]BIO@SNS Laboratory, Scuola Normale Superiore, Pisa, Italy

[8]Section of Human Physiology, Department of Neuroscience and Rehabilitation, University of Ferrara, Ferrara, Italy

[9]Department of Research & Development, Chiesi Farmaceutici, Parma, Italy

Correspondence
Silvia Marinelli, European Brain Research Institute-Fondazione Rita Levi-Montalcini, Via Regina Elena 295, 00161 Roma, Italy.
Email: s.marinelli@ebri.it

Abstract

Background and Purpose: Retinal ganglion cells (RGCs) are the output stage of retinal information processing, via their axons forming the optic nerve (ON). ON damage leads to axonal degeneration and death of RGCs, and results in vision impairment. Nerve growth factor (NGF) signalling is crucial for RGC operations and visual functions. Here, we investigate a new neuroprotective mechanism of a novel therapeutic candidate, a p75-less, TrkA-biased NGF agonist (hNGFp) in rat RGC degeneration, in comparison with wild type human NGF (hNGFwt).

Experimental Approach: Both neonate and adult rats, whether subjected or not to ON lesion, were treated with intravitreal injections or eye drops containing either hNGFp or hNGFwt. Different doses of the drugs were administered at days 1, 4 or 7 after injury for a maximum of 10 days, when immunofluorescence, electrophysiology, cellular morphology, cytokine array and behaviour studies were carried out. Pharmacokinetic evaluation was performed on rabbits treated with hNGFp ocular drops.

Results: hNGFp exerted a potent RGC neuroprotection by acting on microglia cells, and outperformed hNGFwt in rescuing RGC degeneration and reducing inflammatory molecules. Delayed use of hNGFp after ON lesion resulted in better outcomes compared with treatment with hNGFwt. Moreover, hNGFp-based ocular drops were less

Antonino Cattaneo, Scuola Normale Superiore, BIO@SNS Laboratory, Scuola Normale Superiore, Piazza dei Cavalieri 7, 56126 Pisa, Italy.
Email: antonino.cattaneo@sns.it

algogenic than hNGFwt. Pharmacokinetic measurements revealed that biologically relevant quantities of hNGFp were found in the rabbit retina.

Conclusions and Implications: Our data point to microglia as a new cell target through which NGF-induced TrkA signalling exerts neuroprotection of the RGC, emphasizing hNGFp as a powerful treatment to tackle retinal degeneration.

KEYWORDS
hNGFp, microglia, NGF, retinal degeneration, retinal ganglion cells

1 | INTRODUCTION

The retina comprises several neural layers, lined on the outer side by the retinal pigment epithelium (Gupta et al., 2016). Among them, the ganglion cell layer (GCL) contains the cell bodies of retinal ganglion cells (RGCs), and their axons form the optic nerve (ON), the main target of degeneration in ocular diseases.

Among different factors and neurotrophins that modulate the functions of the retina in early post-natal development as well as during the entire life, **nerve growth factor** (NGF) has been widely investigated (Carmignoto et al., 1991; von Bartheld, 1998). Like other neurotrophins, NGF is locally produced in the retina (von Bartheld, 1998). The mature form is derived from its precursor proNGF, following proteolytic cleavage that occurs either intracellularly or within the extracellular space (Bruno & Cuello, 2006), when it activates two distinct cell surface receptors, the **receptor tyrosine kinase 1** (TrkA), triggering different signalling pathways related to cell survival, proliferation and differentiation and the **p75 neurotrophin receptor** (p75NTR). The precursor form proNGF preferentially binds to p75NTR, where signalling has been engaged/implicated in neuronal cell death (Blöchl & Blöchl, 2007; Chao, 2003). The levels of TrkA versus p75NTR signalling and ratio of NGF to proNGF expression are crucial points in determining opposing outcomes of signalling from this ligand–receptor system (Conroy & Coulson, 2022).

The physiological localization of NGF/proNGF and TrkA/p75NTR expression in the rodent retina has been hotly debated, because the results are strongly influenced by the animal model examined, the developmental stage and the tools used for their detection. Moreover, the lesion itself or the inflammatory state of the retina may influence the TrkA/p75NTR receptor cell-type distribution. For instance, immunohistochemical studies provide contradictory results and often due to inadequate specificity of the primary antibodies commercially available (Garcia et al., 2017). In particular, the expression of the TrkA receptor in rats has been attributed to RGCs during embryonic and postnatal stages (Zanellato et al., 1993), whereas other reports showed almost undetectable levels of TrkA expression by RGCs under physiological conditions (Garcia et al., 2017). Single-cell RNA-seq revealed Ntrk1 (TrkA) mRNA expression in a specific RGC subtype and microglia of both human and mouse cells (Benhar et al., 2023; CZI Single-Cell Biology Program et al., 2023; Tran et al., 2019).

What is already known

- NGF has a neuroprotective effect on RGC degeneration.

What does this study add

- NGF-induces RGC neuroprotection by acting on microglia cells.
- hNGFp has superior neuroprotective properties and does not induce eye pain compared with NGF.

What is the clinical significance

- An eye drop hNGFp formulation would improve patient compliance and increase its therapeutic index.
- hNGFp is new neuroprotective therapeutic approach based on a novel mechanism involving retinal microglia.

NGF activity has been investigated in several different models of retinal injury and disorders. For example, NGF recovered RGC function in an animal model of ocular ischemia, reduced retinal injury caused by intraocular hypertension and slowed down retinal degeneration in rats affected by retinitis pigmentosa (Lambiase et al., 1997; Lambiase & Aloe, 1996; LaVail et al., 1992; Mey & Thanos, 1993; Siliprandi et al., 1993). In other preclinical animal models, NGF eye drops or intravitreal injections prevented RGC loss and improved RCG survival (Colafrancesco et al., 2011; Guo et al., 2020). Importantly, murine NGF-mediated protective effects were observed in human patients affected by optic pathway glioma or glaucoma, in which murine NGF administered as eye drops improved visual function (Falsini et al., 2016; Lambiase et al., 2009).

Notably, a recombinant human NGF (hNGFwt)-based ophthalmic eye drop formulation is currently an approved drug (Oxervate®/cenegermin) for the treatment of neurotrophic keratopathy (Hamrah

et al., 2022). To gain access to the retina, higher doses of hNGFwt are typically required, with respect to those doses used for its uses in external eye ophthalmic indications such as neurotrophic keratopathy. Despite a positive safety profile, clinical doses of NGF are hampered by its well-established algogenic effects on the pain system (Pezet & McMahon, 2006), after systemic (Apfel et al., 2000), intracerebroventricular (Eriksdotter Jönhagen et al., 1998) or ocular delivery (Sacchetti et al., 2020). Also, the clinical uses of NGF are limited by its binding to proapoptotic p75NTR receptors. To overcome these pitfalls, that is, its negative effects through p75NTR and pain as dose-limiting adverse side effects, a mutant of NGF (called hNGFp) has been developed. Inspired by the human painlessness genetic disease Hereditary Sensory and Autonomic Neuropathy type V (HSAN V) (Capsoni, 2014; Einarsdottir et al., 2004), hNGFp has similar neurotrophic activity to that of hNGFwt but its pain-sensitizing activity is at least tenfold lower, thus largely increasing its therapeutic window (Capsoni et al., 2011; Malerba et al., 2015). From a pharmacological point of view, hNGFp is a biased agonist of the TrkA receptor in that it effectively binds and activates TrkA, with an identical binding affinity to that of hNGFwt, whereas its binding affinity to p75NTR is almost 200-fold reduced (Covaceuszach et al., 2010). Thus, hNGFp can be considered a painless and p75NTR-sparing hNGF signalling protein.

Retinal microglia play active roles in maintaining the normal structure and functioning of the retina and, importantly, are involved in the refinement of retinal circuitry during development (Silverman & Wong, 2018). Microglial-dependent apoptosis of RGCs and the elimination of unuseful and overnumbered neural connections play a crucial role in the normal postnatal development of the retina and cortical visual areas (Bodeutsch & Thanos, 2000; Schafer et al., 2012).

Being the resident immune cells of the retina, microglia are pivotal under pathological conditions in orchestrating neuroinflammatory responses (Rathnasamy et al., 2019). Upon acute insults, microglia-mediated neuroinflammation promotes neuroprotection and regenerative processes for restoring tissue homeostasis (Bellver-Landete et al., 2019; Gupta et al., 2018). However, under chronic conditions when the insult persists, such as in retinal degenerative disorders, microglia become pathologically activated and release exaggerated amounts of inflammatory mediators that promote tissue damage and cause disease exacerbation, thus affecting visual function (Chen & Xu, 2015; Gupta et al., 2003; Kumar et al., 2023; Margeta et al., 2022; Zhao et al., 2015). Hence, modulation of microglial reactivity represents a rational and well-validated therapeutic approach to attenuate neuronal loss and slow down the progression of retinal degenerative diseases.

Our recent findings in the brain demonstrate that microglia are a new target cell through which NGF induces neuroprotection, by steering these immune cells to a homeostatic phenotype (Capsoni et al., 2017; Rizzi et al., 2018). Altogether, this body of evidence prompted us to investigate the cellular mechanism of hNGFp-mediated neuroprotection in neonatal and adult retinal lesion models.

The present study provides the first evidence that hNGFp rescues RGC degeneration by acting on TrkA expressed by retinal microglia. Moreover, hNGFp appeared more powerful than hNGFwt. These results introduce the proposed clinical use of hNGFp as an effective painless, TrkA-based and p75-less therapy with a higher therapeutic index for visual impairment in retinal neurodegenerative diseases.

2 | METHODS

2.1 | Animals

Long Evans rats and C57BL/6J mice were purchased from Charles River Laboratories (Italy) and bred in the laboratory animal house. Birth is depicted as P0. Rats of both sexes at P2 were used for all experiments on neonates, apart from electrophysiology on isolated retinae in which C57BL/6J mice of both sexes at P2–P3 were used. For immunofluorescence assays with the anti-TrkA receptor mAb MNAC13, CX3CR1$^{GFP/+}$ mice and NTRK1$^{-/-}$ mice were employed. Ocular pain assessment was carried out on 6- to 7-weeks old male C57BL/6 mice. Regarding experiments in adult animals, Sprague Dawley male rats, 180–200 g, 6–7 weeks (Charles River Laboratories, Milan, Italy), were used. Animal studies are reported in compliance with the ARRIVE guidelines (Percie du Sert et al., 2020) and with the recommendations made by the *British Journal of Pharmacology* (Lilley et al., 2020).

Animals were randomized and coded to reduce the risk that people carrying out behavioural analysis, tissue processing and statistical analysis may consciously or subconsciously influence the outcome. Randomization was carried out using the Research Randomizer Program online (www.randomizer.org). The GPower program was used to calculate a priori the sample size. Power, alpha and effect size were set at 80%, 0.05 and 0.44, respectively. The number of subjects in the experiments is reported in the figure legends. All experiments in vivo in the animal husbandry were performed according to the national and international laws for laboratory animal welfare and experimentation (EU directive n. 2010/63/EU and Italian DL n. 26 04/03/2014) and conducted according to the ARVO Statement for the Use of Animals in Ophthalmic and Vision Research. Animals were kept under a 12-h dark to light cycle, with food and water ad libitum. Long Evans rats: authorization n° 633/2018-PR of the Italian Ministry of Health; C57BL/6J mice: authorization n° 233/2017-PR and #94/2015-PR of the Italian Ministry of Health; Sprague Dawley rats: research permits #53/2018-PR and #239/2021-PR, NTRK1 mice: #45/2019-PR.

For pharmacokinetic assessments, all the environmental conditions, animal care and all the procedures adopted throughout the study for housing and handling the animals used as test systems were in strict compliance with EC and Italian Guidelines for Laboratory Animal Welfare (EU 2010/63 Directive and Italian Legislative Decree 2014/26, respectively), formerly approved by the Institutional Animal Welfare Body, and regularly authorized by the national Competent Authority (Italian Health Ministry Authorization

#200/2015-PR dated 31 March 2015). ON models were ON lesions in neonate rats and ON crush injuries in adult rats. Neonatal and adult optic crush rat models were employed in this study to evaluate the neuroprotective, pharmacological and toxicological effects on RGC neurodegeneration of clinical grade molecules, hNGFp and hNGFwt. The crush of the ON is a general model exploited to study mechanisms underlying specific ocular diseases or optic neuropathies, in which the RGC death is a common outcome (e.g. glaucoma, optic pathway glioma, demyelinating optic neuritis, ischemic optic neuropathy and hereditary optic neuropathy). This in vivo experimental system in rats replicates aspects of the human RGC degeneration (PMID: 22603978).

2.1.1 | Optic nerve lesion in neonate rats

To induce ON lesion, neonatal rat pups (P1) of both sexes were anaesthetized by hypothermia (−20°C, 1 min/g; Danneman & Mandrell, 1997). For surgery, animals were placed over a custom-made frozen platform. Surgery was performed under a surgical microscope (Leica Microsystems, Wetzlar, Germany) using a magnification factor of 160× and an operating distance of 20 cm. First, the skin overlying the skull was opened at the midline via a scalpel blade incision followed by opening of a small window in the skull by an almost tangential cut using a scalpel blade, avoiding lesion of the dura. The window was located right behind the bregma, lateral to the midline. After flipping the skull window, a small brain portion was gently removed using a metal 22-gauge cannula with a flat mouthpiece attached to a surgical aspiration pump. This was continued until the skull floor plate was reached and part of the ON, going from the nerve exit of the optic foramen towards the optic chiasm, became visible. The nerve was then cut right behind the foramen using the same suction pipette. Assurance that this nerve was indeed the ON could easily be achieved since movement of the proximal nerve stump could be observed when gently pressing the eye bulb inward. To finish, the skull window was relocated into the place and the skin was sutured. The entire surgical procedure took only a few minutes. Animals were placed in a recovery cage with a heating pad and were given a subcutaneous injection of **carprofen** (5 mg/kg) to provide postoperative analgesia.

2.1.2 | Optical nerve crush injury in adult rats

To perform optical nerve crush injury (ONC), rats were anaesthetized with a mixture of **ketamine** and **xylazine** (90 and 3 mg/kg, respectively, intraperitoneal, i.p.), and the ON was accessed by an incision in the conjunctiva temporally around the eye, which was gently retracted forward using forceps, thus exposing the ON. The left ON was crushed at 0.5 mm from the optic disk for 10 s, applying a constant and consistent force using cross-action forceps. All procedures were performed on the left eye under aseptic conditions. ONC was induced in the left experimental eye, whereas the right eye (sham, unlesioned) served as an internal control. Before and after the

procedure, the eye fundus was observed through the operating microscope to assess the integrity of the retinal blood flow (Galvao et al., 2015). Animals were killed under anaesthesia by beheading at baseline or 4, 7 and 14 days post-injury.

2.2 | Pharmacological treatments

2.2.1 | Intravitreal injection in neonates

Immediately after ON lesion, both control (unlesioned) and lesioned rat pups were subjected to an intravitreal (ivt) injection (250 nL) of either vehicle [phosphate buffered saline (PBS)], hNGFwt or hNGFp solutions. The concentrations of hNGFwt and hNGFp were either 2, 1.5 or 1 μg/mL in PBS. After recovery, pups were returned to their mother. The same doses were ivt injected 12 h post-surgery. Finally, 12 h later (i.e. 24 h after nerve section), pups (P2) were killed by beheading and retinae were collected. For ivt injections, we used a disposable glass micropipette (typical pipette tips were about 30–40 μm) attached to a hydraulic injection system consisting of a plastic tube connected to a Hamilton syringe driven by a digital Harvard apparatus (PHD 2000). Animals received an ivt injection of 250 nL under hypothermic anaesthesia (−20°C). The injection was performed under the surgical microscope and visually monitored by following the movement of the meniscus between the injected solution and the oil of the hydraulic pressure system against a calibrated grid on the microscope eyepiece lens. Injection micropipettes were changed when changing the solution to be injected, and whenever necessary.

2.2.2 | Intravitreal injection in adult rats

Immediately after ONC lesion, both eyes from the same animal (left eye: lesion; right eye: control) received an ivt injection (2 μL) of either vehicle (PBS) or hNGFp solutions. hNGFp concentrations were 0.2, 2 or 20 μg/mL in PBS. hNGFp injections were given once a day, from day 1 to day 4 or to day 7 post-surgery. In another set of experiments, hNGFp injections were given from day 4 to day 7 post-surgery. Eyes and ON were collected immediately after the last treatment, and tissues were processed for immunohistochemistry/immunofluorescence.

2.2.3 | Eye drop administration

hNGFp (0.2, 2, 20 and 200 μg/mL) was administered daily by eye drop (25 μL), one, two or three times per day, starting from day 1 to day 7 post-surgery; in another set of experiments, eye drops were applied from day 4 to day 7 or day 14 post-surgery. hNGFwt (200 μg/mL) was administered daily (one, two or three times per day) starting from day 4 post-surgery. Control rats received the vehicle (25 μL, 0.9% NaCl) in which hNGFp and hNGFwt were dissolved.

Eyes and ON were collected immediately after the last treatment, and tissues were processed for immunohistochemistry/immunofluorescence. For in vivo electroretinographic recordings, rats received eye drop treatment three times per day (8:00 AM, 14:00 PM and 20:00 PM).

2.3 | Eye wiping assay in mice

Ocular instillation (5 μL) of hNGFp and hNGFwt, (all, 0.001, 0.01, 0.1, 1 and 5 μg in 5 μL/eye) or their respective vehicles (isotonic saline, NaCl 0.9% and 1% dimethyl sulfoxide, DMSO) were used to induce an acute nociceptive response as previously described (de Petrocellis et al., 2011). Mice were placed individually inside a Plexiglas chamber and were acclimatized for 20 min before stimulus. The number of eye wiping movements following the drug instillation into the eye was recorded for a 5-min time period and was considered as an index of pungency.

2.4 | Mechanical facial sensitivity

Hypersensitivity to mechanical stimulation of the trigeminal area innervating the eye was tested using the Von Frey filaments (Ugo Basile, Gemonio, Italy) ranging from 0.008 to 0.06 g. Before starting the administration of the neurotrophins, a baseline was recorded for each mouse and subtracted from the values obtained at the end of the treatment.

Following habituation, mice are individually placed in a small transparent cage to allow video recording and presented with a fixed series of von Frey stimuli. The animal's response to each stimulus is scored by measuring the number of times they withdrew their head.

hNGFwt (n = 29) and hNGFp (n = 25) were administered to male C57BL/6J mice via ocular drops at the dose of 0.21 μg/eye. The proteins were diluted in 3 μL of sterile vehicle (bidistilled H_2O) and administered daily for 1 week. As control treatments, mice (n = 25) were treated with vehicle.

2.5 | Production and purification of hNGFwt and hNGFp

Mature hNGFwt and hNGFp were prepared from their precursor forms, hproNGFwt and hproNGFp, produced in *E. coli* solubilized from inclusion bodies, renaturated and purified by two chromatography steps. The hproNGFwt and hproNGFp were then proteolytically cleaved by trypsin by two different protocols, in order to obtain the corresponding mature hNGFwt and hNGFp proteins (Malerba et al., 2015).

In detail, *E. coli* cells, strain Rosetta (DE3) pLysS, were transformed by the plasmids pET11a containing the cDNA sequence of hproNGFp or hproNGFwt. The protocol for growth, expression and purification was the same for the two versions of hproNGF (i.e. hproNGFwt and hproNGFp). Cells were grown aerobically at 37°C in Luria-Bertani broth containing ampicillin (100 mg/L) and chloramphenicol (34 mg/L) until a 600-nm optical density of 0.9–1.0. The expression of hproNGF was induced by addition of 1-mM IPTG (isopropyl thio-β-*D*-galactopyranoside) and subsequent growth for further 4 h. Cells were harvested by centrifugation, lysed and inclusion bodies were isolated and solubilized as in Rattenholl et al. (2001). After the refolding step, the sample was dialyzed against 50-mM sodium phosphate buffer (PB) pH 7 and purified by two subsequent chromatography steps (a cation exchange and a hydrophobic interaction) in an AKTA Purifier system (GE Healthcare, Milano, Italy).

Mature hNGFwt was obtained by a controlled digestion with trypsin (Roche, Monza, Italy; trypsin:proNGF ratio of 1:500, proNGF concentration 0.5 mg/mL) for 3 h at 30°C, whereas hNGFp was cleaved by trypsin (Promega Corporation, Madison, USA; trypsin:proNGF ratio of 1:250, proNGF concentration 0.5 mg/mL), for 14–16 h at 4°C under very low stirring (50 rpm). The corresponding mature NGF forms were then purified by a cation exchange in an AKTA Purifier system (GE Healthcare, Milano, Italy). Fractions containing the protein were pooled and checked by SDS-PAGE and ELISA. The protein manufacturing method has been scaled-up to the scale of 10 L/batch (Malerba et al., 2015). The hNGFp yield after proteolytic cleavage is 1.1 mg/L with a purity of 95.5%, checked by HPLC and mass spectrometry. hNGFwt yield is 16 mg/L (Malerba et al., 2015). All the NGF batches were tested by the TF1 proliferation assay, a quantitative bioassay to determine the potency of NGF and its derivatives (Malerba et al., 2015).

2.6 | MNAC13 anti-TrkA antibody production and purification

Anti-TrkA mAb MNAC13 mouse hybridoma cells were cultured and purified as described in Cattaneo et al. (1999). MNAC13 batches were tested by ELISA, SDS-PAGE and by a specific TF1 bioassay, as described in Malerba et al. (2021).

2.7 | Retinal immunofluorescence and immunohistochemistry

2.7.1 | Immunofluorescence from neonate rat samples

All immunofluorescence experiments from neonate rats were performed on whole-mount retinae. Animals (P2) were killed by decapitation followed by rapid enucleation of the eyes, which were then fixated in 4% paraformaldehyde in PBS (sc-281692, Santa Cruz Biotechnology, Heidelberg, Germany) for 1 h at room temperature (RT). Afterwards, eyes were transferred to a 30% sucrose solution (S0389, Sigma-Aldrich, Darmstadt, Germany) in 0.1 M PB. Retinae were then

dissected as flat mounts and four cuts were made to delimitate the four quadrants. Whole-mount retinae were put in 10-mM citrate buffer (pH 6.0; P4809, Sigma-Aldrich, Darmstadt, Germany) for 15 min at 95–100°C. After washing 3× for 10 min in PB 0.1 M, retinae were blocked overnight at 4°C in a PB solution containing 5% normal donkey serum (NDS, 566460, Sigma-Aldrich, Darmstadt, Germany) and 0.5% Triton X-100 (93443, Sigma-Aldrich, Darmstadt, Germany). This was followed by incubation of the samples for 5 days at 4°C in a PB solution containing 5% NDS and 0.5% Triton X-100 as well as with the following primary antibodies: 1:500 anti-RBPMS (RGC marker, raised in guinea pig, 1832-RBPMS, PhosphoSolutions, Aurora, USA, RRID:AB_2492226), 1:1000 monoclonal anti-MNAC13 antibody (TrkA-receptor, mouse; Cattaneo et al., 1999), 1:500 anti-Iba1 antibody (microglia marker, raised in rabbit, 019-19741, Wako, Richmond, USA, RRID:AB_839504) and 1:300 anti-rat CD68 (raised in mouse, MCA341R, Serotec, Neuried, Germany, RRID:AB_2291300). On the sixth day, samples were washed 3× for 10 min in PB 0.1 M and incubated with the appropriate secondary antibodies: goat anti-guinea pig Alexa 647 (A21450, Thermo Fisher, Waltham, USA, RRID:AB_2535867), goat anti-mouse Alexa 555 (A32727, Thermo Fisher, Waltham, USA, RRID:AB_2633276) and goat anti-rabbit Alexa 488 (A32731, Thermo Fisher, Waltham, USA, RRID:AB_2633280) diluted in a PB solution containing 0.3% Triton X-100 and 5% NDS as follows: 1:700 for 2 days at 4°C. Retinae were then washed 3 times for 10 min in PB solution, after which **DAPI** staining (1:1000, D9542 Sigma-Aldrich, Darmstadt, Germany) was performed overnight at 4°C in a PB solution with 0.3% Triton X-100. The day after, retinae were washed 3× for 10 min in PB solution and mounted on glass slides in Vectashield (H1000, Vector Laboratories, Newark, USA) and cover slipped.

2.7.2 | Immunofluorescence and immunohistochemistry from adult rat samples

For paraffin-embedded sections, anaesthetized rats were perfused transcardially with PBS and 4% paraformaldehyde, eyes and ON were collected, postfixed for 24 h and paraffin-embedded. Paraffin sections (5 μm) were placed on a hot plate to allow sections to adhere to the slide; deparaffinization and rehydration of the sections were performed by sequential incubations in xylene and descending ethanol series (100%, 90%, 70% and 30%). Antigen retrieval was performed with a 10-mM citrate buffer (pH 6.0) for 9 min at 90°C for retinal sections and with a 10-mM citrate buffer (pH 6.0) for 20 min at 99°C for nerve sections. Sections were incubated with the primary antibodies Iba-1 (1:1000, 013-27691 Wako, Richmond, USA, RRID:AB_2934095), OX-6 (1:200, 554926 BD Pharmingen, San Diego, USA, RRID:AB_395603) and GAP-43 (1:3000, ab75810 Abcam, Cambridge, UK, RRID:AB_1310252) diluted in PB solution containing 5% normal goat serum (NGS, S26-M, Sigma-Aldrich, Darmstadt, Germany) for 1 h at RT in a humidity chamber. Sections were then incubated with fluorescent secondary antibodies: polyclonal Alexa

Fluor 488 and polyclonal Alexa Fluor 594 (1:600, A32731, goat polyclonal anti-rabbit and A11005, goat polyclonal anti-mouse, Invitrogen, Waltham, USA, RRID:AB_2633280 and RRID:AB_2534073 respectively) 2 h at RT, protected from light. Sections were coverslipped using a mounting medium with DAPI (ab104139, Abcam, Cambridge, UK). Tissues were visualized, and digital images were captured using a Zeiss AxioImager2 microscope in z-stack and Apotome mode (Carl Zeiss Spa, Milan, Italy). Iba-1 and OX-6 counting was performed in all retinal layers. Cell number was counted in three to five consecutive fields (40× magnification) of three different sections for each eye.

For immunohistochemistry, some sections were stained with haematoxylin and eosin (H&E) for histological examination. Other sections were incubated with the primary antibody RBPMS (1:500, 1832 PhosphoSolutions, Aurora, USA, RRID:AB_2492226) diluted in PB solution containing 5% normal goat serum (NGS, S26-M, Sigma-Aldrich, Darmstadt, Germany) for 1 h at RT in a humidity chamber, after antigen retrieval with a 10-mM citrate buffer (pH 6.0) for 20 min at 99°C and then incubated with a biotinylated secondary antibody anti-guinea pig (1:200, BA-7000, Vector Laboratories, Newark, USALabVision) for 2-h incubation. Staining was achieved using Avidin-Biotin-Peroxidase (ABC) (1:100, PK-6100, Vector Laboratories, Newark, USALabVision). Signal was detected using 3.3′diaminobenzidine (SK-4105, Vector Laboratories, Newark, USALabVision) as a chromogen. Nuclei were counterstained with Mayer's haematoxylin. After selection at low power magnification of immuno-positive cells, RBPMS+ cells and the total number of cells in the GCL were counted in six to eight random high-power fields (HPF, X400, Leica Microsystem, Wetzlar, Germany). For cryosections, anaesthetized rats were perfused trans-cardially with PBS and 4% paraformaldehyde; eyes were collected, postfixed for 24 h and preserved in sucrose (30%). Cryosections (10 μm) were blocked with 5% normal goat serum (NGS, S26-M, Sigma-Aldrich, Darmstadt, Germany) diluted in PB + triton 0.3% for 1 h at RT followed by the incubation with primary antibodies RBMPS (1:500, 1832 PhosphoSolutions, Aurora, USA, RRID:AB_2492226), IL-1β (1:100, NB600-633 Novus Biologicals, Centennial, USA, RRID:AB_10001060), TNF-α (1:200, NBP1-19532 Novus Biologicals, Centennial, USA, RRID:AB_1643202) and IL-6 (1:400, NB600-1131 Novus Biologicals, Centennial, USA, RRID:AB_10001997). Sections were then incubated with fluorescent secondary antibodies polyclonal Alexa Fluor 488 and polyclonal Alexa Fluor 594 (1:600, A32731, goat polyclonal anti-rabbit; A11005, goat polyclonal anti-mouse and A11076, goat polyclonal anti-guinea pig, Invitrogen, Waltham, USA, RRID:AB_2633280 and RRID:AB_2534073 respectively) 2 h at RT, protected from light. Sections were coverslipped using a mounting medium with DAPI (ab104139, Abcam, Cambridge, UK). Tissues were visualized, and digital images were captured using a Zeiss Axio Imager 2 microscope with Z-stacks in the Apotome mode (Zeiss, Oberkochen, Germany). **IL-1β**, **IL-6** and **TNF-α** staining were evaluated as the fluorescence intensity measured by the microscope program ZEN 2.6 blue edition (Zeiss, Oberkochen, Germany).

2.8 | Axon outgrowth measurement

The ON was immunoassayed for GAP-43 and analysed using a fluorescence microscope (BX63, Olympus, Tokyo, Japan). For analysis, the centre of the field of a 40× magnification objective lens was positioned at 0.25, 0.50, 0.75, 1.00, 1.50 and 2.00 mm from the proximal border of the crush site. At each point, a blinded observer counted the number of GAP-43+ axons and measured the cross-sectional width of the nerve, in five longitudinal sections. The values obtained represented the total number of axons per nerve at each distance from the lesion site.

2.9 | Confocal microscopy

Analysis by structured illumination microscopy (SIM) of the flat-mounted neonatal retinae was performed using an X-light V2 confocal spinning disk system fitted with a Video Confocal super-resolution module (CrestOptics, Italy) equipped with a 40×/1.25 NA PlanApo Lambda oil immersion objective (Nikon, Japan), a Zyla sCMOS camera (Andor) and Spectra X Lumencor LEDs Light Source with bandpass excitation filters of 460–490 and 535–600 nm (Chroma Technology, US). For each sample field, all the channels (green: Alexa Fluo 488; red: Alexa Fluo 555; far red: Alexa Fluo 647, DAPI) were simultaneously acquired. The SIM raw data with 16-bit depth was computationally reconstructed, channel specifically, using the Metamorph software package.

2.10 | Cell counts

Cell counts were obtained from confocal stacks through the entire RGC depth (13 to 25 planes) and were performed at fixed locations in the retina in 187.5 μm × 187.5 μm square fields (40× zoom 2×). Each field was analysed to evaluate the presence of RBPMS+, MNAC13+, Iba1+ and CD68+ cells. Cell counts were performed going from the upper left corner towards the lower right corner. DAPI staining was used as a nuclear marker to identify healthy from apoptotic RGCs. Total cell counts per retina were obtained by averaging the cell densities (cell/mm^2) obtained in the retinae and multiplying this average density by the retinal area (mm^2). Retinal areas were measured on their image TIFF files using the ImageJ Software. Cell counts were performed blind to the treatment condition.

2.11 | Microglia morphological analysis

Morphometric analysis was performed as previously shown (Marrone et al., 2017) and obtained from confocal stacks through the entire retinal thickness, at fixed locations in the retina in 187.5 μm × 187.5 μm square fields (40× zoom 2×). Confocal stacks were used to produce the maximal projection images that were analysed with plugin 'Shape descriptor 1u' of Image J software (http://imagej.nih.gov/plugins) as follows: images were reduced at 8 bit from the original RGB acquisition, and a threshold was established to obtain a digital image where neither the original signal disappeared nor new signal was created. The analysis was performed automatically on cell silhouettes, going from the upper left corner towards the lower right corner, and the following parameters were measured: area (A, μm^2), perimeter (P, μm) and circularity ([4π × [area (μm^2)]/[perimeter (μm)]^2). The circularity (2D value) of a cell is defined as the entire periphery of a planar figure. A value of 1, for the 'circularity' index, indicated a perfect circle, whereas a value approaching 0 represented an increasingly elongated shape; thus, a more ramified cell will have a smaller circularity value than an amoeboid one. As an index of microglia morphology, we considered the transformation index (TI) (Marrone et al., 2017) calculated as follows: [perimeter of cell (μm)]^2/4π × [cell area (μm^2)]. This index is a dimensionless number providing a measure of the overall shape and morphological complexity of a cell. A low value corresponds to a more amoeboid, rounded shape, whereas increasing values represent a more ramified morphology. Since TI is dependent on cell shape but is independent of cell size, which is crucial for the identification of different microglia activation states (Marrone et al., 2017), we also employed the area/TI ratio (A/TI) index. Opposite to TI index, a low A/TI value correlates with a more ramified shape, whereas increasing values represent a more ameboid morphology. An additional 'rounded' morphology was visually identified and manually examined, due to its faint staining (Figure 2d).

All the distinct parameters were analysed and compared between lesioned and unlesioned animals, as well as between the four different treatment groups (naïve, vehicle, hNGFwt and hNGFp) at a dose of 1.5 μg/mL (Table 1). Morphological analyses were performed blind to the treatment conditions.

2.12 | Multielectrode array recordings in neonatal retina

Multielectrode array (MEA) recordings were performed by isolating the retina from the mouse pups (P2–P3). Halved retinae were then placed, with the ganglion cell side facing down, on a flat array of 120 extracellular electrodes (Multichannel Systems, Reutlingen, Germany, 120MEA30/10iR-ITO). The retina was superfused with oxygenated Ames' medium (Sigma-Aldrich, Darmstadt, Germany, A1420; equilibrated with 95% O_2 and 5% CO_2 gas) at a flow rate of 2 mL/min at 37°C. Prior to the recordings, retinae were left to acclimatize on the array for at least 15 min. Signals from each electrode were continuously sampled at 25 kHz for 70–150 min (Multichannel Systems, Reutlingen, Germany, MEA2100-System). The spike trains for individual RGCs were extracted via further offline processing with SpyKING CIRCUS (Yger et al., 2018). A total of 28 retina MEA recordings were performed, each containing 30–126 RGCs. Of these

TABLE 1 Graphical summary of microglia cell morphology.

	Unlesioned	Lesioned
Naive	Area 121.5 Circularity 0.206 TI 0.814 A/TI 159.9	Area 182.9 Circularity 0.232 TI 0.680 A/TI 314.7
VEH	Area 154.4 Circularity 0.195 TI 0.751 A/TI 217.4	Area 190.6 Circularity 0.237 TI 0.617 A/TI 359.2
hNGFwt	Area 160.4 Circularity 0.203 TI 0.728 A/TI 242.1	Area 184.7 Circularity 0.230 TI 0.667 A/TI 303.8
hNGFp	Area 168.2 Circularity 0.193 TI 0.690 A/TI 255.1	Area 157.2 Circularity 0.208 TI 0.744 A/TI 232.8

Note: For both unlesioned and lesioned optic nerve animals, values of area, circularity, TI and A/TI are given for all the experimental groups [naïve, vehicle (PBS), hNGFwt and hNGFp]. All values reported in the table represented the average of each group.

28 retinae, hNGFp (100 ng/mL) was added to the bath of 10 retinae for 25–30 min in the middle of the recordings. Six retinae were incubated with an inhibitor of microglia activation, **minocycline** (MI, 100 nM), for at least 1 h prior to addition of hNGFp for 30 min. MI was present throughout the entire recording. Four retinae were incubated with anti-TrkA antibody (1-μg/mL MNAC13) for at least 2.5 h and then examined with hNGFp for 30 min under a continuous flow of the antibody. The last eight retinae were recorded in the absence

of hNGFp, minocycline or MNAC13 to provide a control condition. The retinae were then further processed for immunofluorescence analysis.

The inter-wave intervals (IWIs), as well as the peak average firing rate of the retinal wave (spikes/s/cell), were analysed. For each recording condition, these parameters were analysed and compared during a time window of 20 min.

2.13 | Electroretinogram (ERG) analysis in adult rats

After the end of the eye drop treatment, adult rats underwent dark adaptation overnight in a controlled environment. The following day, they were anaesthetized with an intraperitoneal injection of **sodium pentobarbital** (30 mg/kg) and prepared for the ERG routine consisting of serial recordings of scotopic ERG (scERG), photopic ERG (phERG) and pattern ERG (PERG) using a commercially available recording system (SB700 Advanced, Nikon-Europe, Amsterdam, The Netherlands). The ERG responses were unilaterally recorded from the left eye using an Ag/AgCl corneal electrode and a reference electrode placed on the forehead, while a ground electrode was placed on the tail. The body temperature was maintained at 38°C using a homeothermic controller. Recordings were initially taken in the absence of stimuli, to measure the background noise levels. Light stimuli were calibrated as luminance energy units in candela seconds per metre squared (cd-s/m^2). The scERG was elicited using a 1.00 log cd-s/m^2 stimulus. The deriving waveforms were analysed by considering the amplitude of the a-wave (early negative component) and the b-wave (belated positive waveform) as primary parameters of the scERG response. After the acquisition of the scERG, rats were light-adapted for 10 min before recording phERG using a 3 cd-s/m^2 stimulus on a 30 cd-s/m^2 rod-saturating background light. For each rat, 10 waveforms were recorded with an interstimulus interval of 3 s and averaged. The phERG waveforms were analysed by considering the b-wave amplitude, retrieved from the baseline to the positive peak (due to the typical lack of a consistent a-wave), and the photopic negative response (PhNR), identified as the first negative deflection after the b-wave whose amplitude was considered from the baseline to the belated negative through. Thereafter, rats underwent PERG analysis performed by delivering alternating patterns of black and white horizontal bars with a spatial frequency of 0.05 cycles/deg reversing at 1 Hz and presented at 98% contrast. The pattern stimuli were administered through a light-emitting diode display with a mean luminance of 50 cd/m^2 aligned at about 20 cm from the corneal surface. A total of 300 signals were averaged. The PERG waveform was evaluated by measuring the amplitude of the N35–P50 (from the trough of the negative peak, N35, to the peak of the positive peak, P50) and P50–N95 waves (from the peak of the positive peak, P50, to the trough of the negative peak, N95). The implicit time was determined by measuring the time from the onset of the stimulus to the P50 and N95 peaks.

2.14 | Cytokine measurement

P2 rats (n = 3/group, 6 retinae/group) were killed by decapitation followed by enucleation of the eyes, which were then washed in cold PBS. Retinae were rapidly dissected on ice, pooled together based on the experimental group and rinsed for 40 min in lysis buffer (20-mM Tris–HCl, pH 7.4; 1% TRITON X-100; 150-mM NaCl; 1-mM EDTA; 1-mM EGTA; 1% NP-40; 1% NaDOC; 2.5-mM sodium pyrophosphate; 1-mM Na3VO4) containing a cocktail of protease inhibitors (Complete, Roche Diagnostics, Basel, Switzerland) and phosphatases (Sigma-Aldrich, Darmstadt, Germany). Tissues were sonicated (Vibra-Cell VCX130, Sonics) on ice 20 s, centrifuged at 14,000 rpm for 15 min at 4°C, and the supernatant was collected. Protein concentrations were quantified using the Bradford Assay (Bio-Rad Protein Assay 500–0006, Munchen, Germany).

Concentrations of 27 cytokines were determined using a quantibody rat array kit (#QAR-CYT-3, RayBiotech, GA, USA) in accordance with the provided kit-specific protocols. The following cytokines were measured: beta-NGF, **CD86** (B7-2), **CINC-1** (CXCL1), **CINC-2**, **CINC-3**, **CNTF**, Fractalkine (**CX3CL1**), **GM-CSF**, **ICAM-1** (CD54), **IFN-gamma**, **IL-1 alpha** (IL-1 F1), IL-1 beta (IL-1 F2), **IL-10**, **IL-13**, **IL-2**, **IL-4**, **IL-6**, **LIX**, L-Selectin (CD62L), **MCP-1** (CCL2), **PDGF-AA**, **Prolactin R**, **RAGE**, TCK-1 (**CXCL7**), **TIMP-1**, TNF alpha and **VEGFA**. Briefly, lyophilized rat cytokine standards were first reconstituted with the kit-provided standard diluent, and a standard dilution series was made. Retinal protein lysates were run in duplicate at 1 mg/mL. One hundred microlitres of samples, standards and corresponding buffer blanks were incubated with the array glass slides on a plate shaker at 4°C overnight. After extensive washing, a biotinylated antibody cocktail was added and incubated on a shaker at RT for 3 h. The reaction mixture was detected by the addition of a Cy3dye-conjugated streptavidin following a series of wash steps and incubated on a plate shaker at RT for 1 h. After the washing steps, the array glass slides were carefully air dried and sent to RayBiotech for fluorescence detection through the use of a laser scanner equipped with a Cy3 wavelength (green channel) and data extraction.

2.15 | Ocular pharmacokinetics in rabbits

hNGFp was delivered as topical ocular drops to groups (n = 6–10) of New Zealand White rabbits at doses of 100, 200 and 400 μg/day for 14 days. Low and mid doses were given once a day, whereas the high dose was delivered twice a day, 6 h apart (5 h apart in non-working days). hNGFp was delivered as a ready-to-use solution (1 mg/mL in 10-mM Na acetate buffer, 10-mM methionine, 154-mM NaCl and 0.1-mg/mL polysorbate 80, pH 5.5), and the dosage volume administered to both eyes was 0.05 mL/eye at the low dose and 0.1 mL/eye at the mid and high doses. Plasma, vitreous humor and retina samples were collected on day 14, 24 h after the last administration. Blood samples were collected into K3-EDTA collection tubes. Samples were placed immediately in an ice bath and kept cool until centrifugation (3 min, 10,000 g, +4°C). For each sample, plasma was divided into two aliquots (about 75 μL/aliquot) and stored in a freezer set at −80°C pending analysis. Vitreous humor was collected with a syringe (at least 0.15 mL/aliquot, 3 aliquots/sample), and then the left eye was cut and the retina collected; the retina was washed once with saline solution. Vitreous samples were stored at −80°C and retinae at +4°C, pending analysis. Concentrations of hNGFp in rabbit plasma, vitreous humor and retina homogenate were determined by a validated Luminex® xMAP method in the calibration range 3.2–2000 pg/mL, 6.4–4000 and 9–4000 pg/mL, respectively. The Luminex® xMAP assay kit (Millipore, Burlington, USA, HADK2MAG-61K) is a paramagnetic fluorescent microsphere beads-based assay in which the coloured beads, coated with an anti-human β-NGF antibody, are used to capture the analyte. The bond is then detected using a biotinylated secondary antibody and streptavidin-phycoerythrin as its substrate. The sandwich bound to the coloured magnetic beads was analysed through a fluidic system where light sources excite the internal coloured dye that identifies the microsphere beads as well as the reporter dye phycoerythrin captured during the assay, allowing the direct measurement of the concentration of the test item.

2.16 | Data and statistical analyses

All quantitative analyses were conducted blind to the animal's experimental groups. Outliers were removed following statistical paradigms. Statistical analysis was performed using the GraphPad Prism 5 program. Only one value of P has been used throughout the manuscript ($P < 0.05$). After ANOVA, post hoc tests were run only if F achieved the necessary level of statistical significance (i.e. $P < 0.05$). For neonate samples, data were analysed using two-way ANOVA, followed by Tukey's post hoc tests and unpaired t-tests (Figure 2d). For adult tissues, one-way ANOVA followed by Tukey's test was carried out. For each experiment, data values, means ± SEM, number of samples and statistical analyses, P-values, were collected in the Supporting Information.

MEA recording data were analysed in Matlab (Mathworks) and Python. For each recording, the time histogram of population firing rates (1s bin width) was first computed and individual retinal waves were identified by setting a threshold of 1 spike/s/cell. Then, the (i) IWIs between the peaks and (ii) the peak firing rate averaged over the cells involved in each retinal wave were calculated. For each recording condition, these parameters were compared across the following three time-periods: (i) a 20-min window right before the onset of the hNGFp bath application, (ii) the last 20 min of the hNGFp application period and (iii) a 20-min window starting 10 min after the offset of the hNGFp application. Kruskal–Wallis and Dunn's post hoc tests were performed with a significance set at $P < 0.05$. No statistical method was used to predetermine the sample size.

ERG data were computed and analysed using Prism 8.0.2 (GraphPad Software, Inc., San Diego, CA, USA). Data were tested for

normal distribution using the Shapiro–Wilk normality test. Differences between groups were tested using one-way ANOVA followed by Tukey's multiple comparison post hoc test. All data were expressed as mean ± SEM with statistical significance given at $P < 0.05$.

Multi-array cytokine data have been obtained from biological 4 replicas. Given the numerous missing values obtained, each single Log2-transformed value was normalized by subtracting the median of Fractalkine, ICAM-1 and VEGF of the corresponding sample and adding the median across all samples, since the value of these three cytokines could be reliably measured in all replicas and experimental groups. Cytokine values used for hierarchical clustering and principal component analysis are the average of non-null samples.

2.17 | Materials

Details of materials and suppliers are provided in specific subsections in Methods.
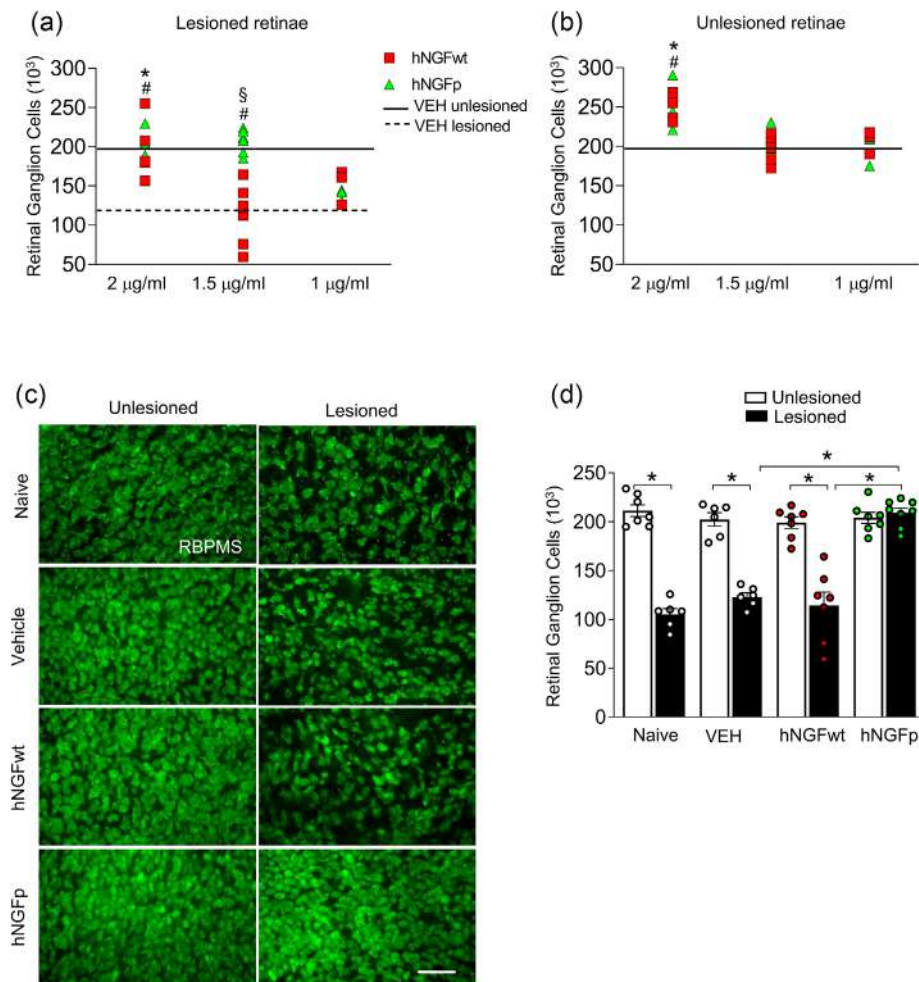
FIGURE 1 At a concentration of 1.5 µg/mL, hNGFp has a superior protective effect over that of hNGFwt on RGCs in a neonatal model of retinal degeneration. (a–b) The graphs represent the total number of RGCs counted in retinae from rats with lesioned (left panel, a) and unlesioned ON (right panel, b) after ivt injections of vehicle (PBS), hNGFwt or hNGFp solutions. Tested concentrations: 2, 1.5 and 1 µg/mL. Solid line: mean value of RGCs from unlesioned ON animals receiving ivt vehicle; dashed line: mean value of RGCs from lesioned ON animals receiving ivt vehicle. Data are expressed as mean ± standard error, n = 6–7/group, except for 1-µg/mL dose; $P < 0.05$; where not specified, statistical comparisons among groups resulted not significantly different ($P > 0.05$). Two-way ANOVA, Tukey's multiple comparisons test * vehicle (PBS) versus hNGFwt; # vehicle (PBS) versus hNGFp; § hNGFwt versus hNGFp. (c) Confocal images from unlesioned and lesioned retinae with RBPMS labelling of RGCs (green), in naïve (no ivt inj), vehicle, hNGFwt and hNGFp ivt delivered. Note that in lesioned retinae ivt injected with PBS or hNGFwt 1.5 µg/mL, RBPMS labelling is reduced, whereas in hNGFp-treated retinae, RBPMS signal is similar to unlesioned retinae. Scale bar: 25 µm. (d) Histograms represented RBPMS+ RGC counts in unlesioned (white) or lesioned (black) retinae from P2 naïve pups (no ivt) or pups treated by intravitreal injection (ivt) with vehicle (PBS), hNGFwt and hNGFp at the dose of 1.5 µg/mL (n = 6–7/group). In control (unlesioned) retinae, any treatment did not influence RGC density ($P > 0.05$; for more details, see the Supporting Information). Conversely, optic nerve lesion induced a significant RGC loss in naïve animals, in PBS- and hNGFwt-treated pups, whereas it did not in hNGFp-treated animals. Mean ± standard error. Two-way ANOVA, Tukey's multiple comparisons test *$P < 0.05$, naïve unlesioned versus lesioned and naïve versus unlesioned treatment.
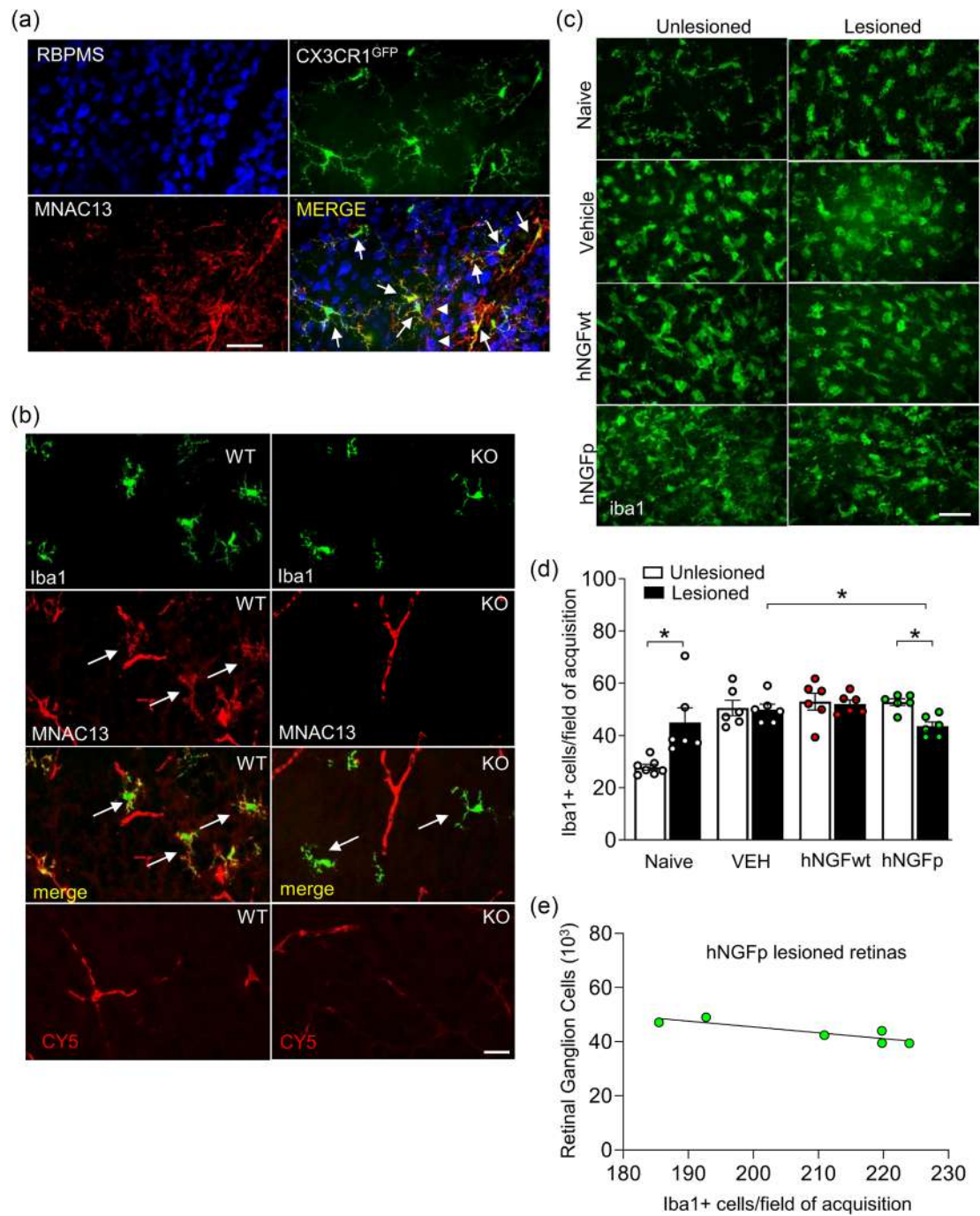
FIGURE 2 Legend on next page.

2.18 | Nomenclature of targets and ligands

Key protein targets and ligands in this article are hyperlinked to corresponding entries in https://www.guidetopharmacology.org and are permanently archived in the Concise Guide to PHARMACOLOGY 2021/22 .

3 | RESULTS

3.1 | Dose–response effect of hNGFwt and hNGFp on RGC degeneration in a neonatal rat optic nerve lesion model

We first tested the effect of hNGFp in a neonatal rat ON lesion model, in which neuroprotection by mouse NGF had been previously demonstrated against RGC death (Rabacchi et al., 1994). Based on that study, we first carried out a pilot dose-finding experiment that allowed us to select intravitreal hNGFp doses in the range of 1–2 μg/mL for later and more in-depth studies.

A head-to-head pharmacological comparison study was then performed on the same model, to comparatively evaluate the dose-dependent effects of intravitreally administered (ivt) hNGFwt and hNGFp on RGCs degeneration.

ON injury significantly decreased the RGC number (Figure 1a–b). Ivt injection of 2-μg/mL hNGFp or hNGFwt in rats subjected to ON lesion significantly reverted the RGC number to that of unlesioned retinae, relative to ivt vehicle (Figure 1a). At this concentration, both hNGFp and hNGFwt enhanced considerably the number of RGCs in unlesioned retinae compared with vehicle-treated controls (Figure 1b), suggesting that both molecules may delay the physiological and developmental RGC death physiologically occurring in neonate rodents (Galli-Resta & Ensini, 1996).

At 1 μg/mL, neither hNGFp nor hNGFwt affected RGC number in both ON unlesioned and lesioned neonatal retinae, in relation to vehicle-treated unlesioned retinae (Figure 1b), pointing out that, at this dose, both drugs do not exert any effects on RGC survival.

Afterwards, we tested 1.5-μg/mL hNGFp and hNGFwt ivt administration. In axotomized retinae, only hNGFp rescued significantly the RGC death induced by ON injury ($206.59 \pm 7.5 \times 10^3$ RGCs in ivt hNGFp lesioned retinas versus PBS-treated unlesioned, $n = 5$, $P = 0.55$), whereas hNGFwt, at the same dose, did not (Figure 1a,c,d). On the other hand, in the unlesioned retina, neither drug affected the number of RGC (Figure 1b; also 1a,c,d). Altogether, these results highlight the 1.5-μg/mL dose of hNGFp as being selectively effective, compared with hNGFwt, indicating a superior pharmacological efficacy. The aforementioned findings also were clearly visible when comparing the confocal images of unlesioned and lesioned retinae, in which a selective recovery of RGCs (identified with the RBPMS marker) in lesioned retinae was observed only following 1.5-μg/mL treatment with hNGFp and not with the same dose of hNGFwt (Figure 1d). Based on these results, the following experiments were consistently performed at the 1.5 μg/mL ivt dose.

3.2 | hNGFp rescued reactive microglia in lesioned neonatal retinae

Our previous evidence in the brain indicates that TrkA receptors are expressed in microglia and their activation by NGF protects neurons by regulating microglial homeostatic activities (Rizzi et al., 2018). We therefore tested if retinal microglia were the target cells of hNGFwt and hNGFp. We investigated the expression of TrkA receptors in the whole-mounted retinae, by using the mouse anti-TrkA monoclonal antibody MNAC13 (Cattaneo et al., 1999). As in the brain, we found that MNAC13 labels microglia in the retina (GFP+ cells; Figure 2a).

FIGURE 2 The TrkA receptor is expressed by retinal microglia and its activation by hNGFp counteracts the increased number of microglia following ON lesion. High-resolution confocal laser scanning photomicrographs of whole-mounted retinae from adult CX3CR1GFP/+ mice (a), and neonatal cortical brain section from wild type (wt) and TrkA ko mice (b, right panels and left panels, respectively), showing the staining pattern of the anti-TrkA MAb MNAC13 (in red). (a) MNAC13 stains mostly GFP+ cell processes and somas (in green, arrows) whereas only rarely it weakly stains also RBPMS+ RGC (in blue, arrowheads); stack bar 20 μm. (b) Specificity of the anti-TrkA Mab MNAC13. Representative wt and KO sections showing Iba1+ microglia (green), MNAC13 staining pattern (red) and their merge (yellow). Note that the TrkA signal on microglia cells (see arrows) from KO tissue disappears. The residual MNAC13 labelling in TrkA KO tissue is related to the background controls of the secondary anti-mouse IgG antibody (CY5) and are most likely blood vessels, since P2 mice could not be perfused transcardially. White arrows indicate microglia cells. CX3CR1GFP+ mice n = 3; Ntrk1tm1Bbd/J (TrkA ko) mice n = 3. (c,d) At the concentration of 1.5-μg/mL dose, only hNGFp decreased the enhancement of microglia induced by enhancement in lesioned retinae. (c) Confocal images from unlesioned and lesioned retinae with Iba1+ labelling. Scale bar: 25 μm. (d) Histograms represented Iba1+ (microglia marker) cell counts in unlesioned (control, white) or lesioned (black) retinae from P2 naïve pups (no ivt), pups treated by intravitreal injection (ivt) of PBS (vehicle), hNGFwt or hNGFp at the dose of 1.5 μg/mL (n = 5/group). Optic nerve lesion markedly increased Iba1+ cells in naïve retina (n = 6/group, P < 0.05). Similarly, in the unlesioned, ivt injection per se significantly enhanced Iba1+ cells (P < 0.05 unlesioned ivt injected versus unlesioned naïve), whereas PBS- and hNGFwt-treated lesioned retinae showed a comparable Iba1+ cell amount to their respective unlesioned controls (n = 6, P = 0.43). hNGFp treatment reduced considerably microglial cell number in lesioned retinae (P < 0.05). Mann–Whitney test and unpaired t-test. Mean ± standard error. (e) The number of RGC and microglia upon hNGFp treatment were negatively correlated. Scatter plot showing the relationship between the number of RGCs and Iba1+ cells from lesioned retinae of mice treated by ivt injection of hNGFp at the dose of 1.5 μg/mL (n = 6/group) P < 0.05 (r = −0.8769). Pearson correlation's coefficient was used for correlation analysis.
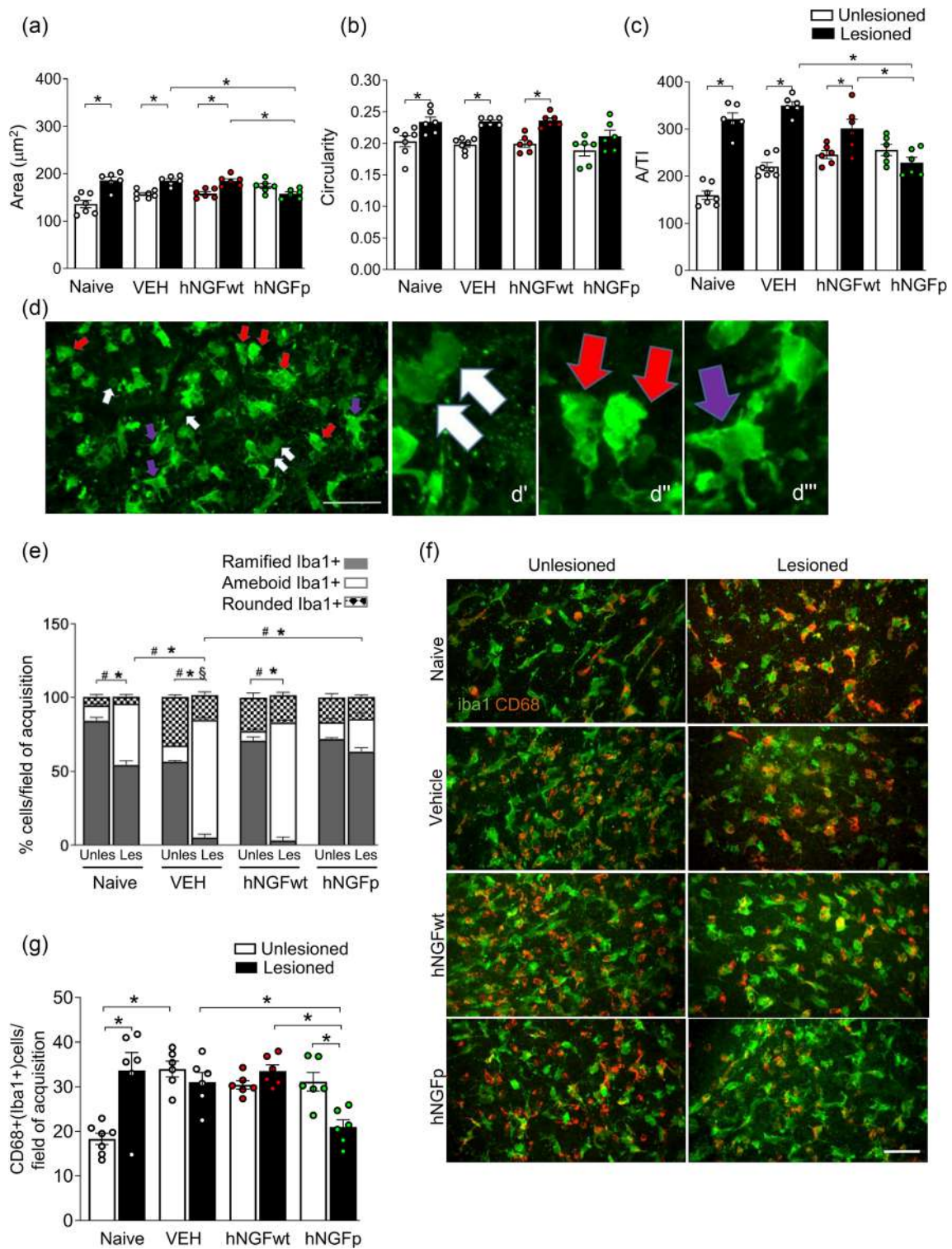
FIGURE 3 Legend on next page.

Although most of the RBPMS+ cells do not exhibit MNAC13 signal, some RBPMS+ cells do show a weaker MNAC13 signal (arrowheads in Figure 2a), which could be due to (i) bonafide low TrkA expression in some ganglion cells or to (ii) microglia processes, not filled by GFP microglia reporter, surrounding RGCs. The specificity of mAb MNAC13 was assessed in tissue from TrkA knockout (KO) mice (Smeyne et al., 1994) (Figure 2b).

Altogether, these data demonstrate that TrkA is expressed by microglia in the retina, as in the brain, and that the aforementioned neuroprotective effect of hNGF on RGC might be reached mostly through microglial modulation.

Under pathological conditions, microglial cells become reactive and rapidly change their morphology, number and phenotype based on surrounding signals from damaged cells. In the present study, ON lesion triggered an increase in the number of retinal Iba1+ cells in naïve rats (Figure 2c–d). We also observed a significant enhancement of microglia cell number following ivt injection of PBS, hNGFwt or hNGFp in unlesioned retinae, indicating that the ivt injection per se enhanced microglial cell number (Figure 2c–d). In lesioned retinae, neither ivt PBS nor 1.5-μg/mL hNGFwt affected microglia cell number, whereas 1.5-μg/mL hNGFp significantly reduced the elevated number of microglia induced by ON lesion (Figure 2c–d). These data pointed out that, at the 1.5-μg/mL dose, only hNGFp (and not hNGFwt) reduced the microglia increase and only after ON lesion. This suggests a lesion-induced responsiveness of microglia to hNGFp.

A clear link between microglia and RGCs may underpin the neuroprotective efficacy of hNGFp, as evidenced by the negative correlation between the number of microglia cells and RGCs in lesioned retinae treated with hNGFp (Figure 2e).

Since microglial density, morphology and function are strictly interrelated, morphological changes being predictive of functional alterations (Davis et al., 1994), we analysed microglia morphology (see Methods) in retinae from both ON lesioned and unlesioned neonate rats, receiving or not pharmacological treatments (Table 1 and Figure 3). The ON lesion caused a significant increase in the overall microglial cell area, circularity and A/TI ratio in naïve, PBS- and hNGFwt-treated groups, with the exception of hNGFp-treated rats (Figure 3a–c). These results show that morphological changes induced by ON lesion were rescued by hNGFp alone, steering microglia morphology from a round, ameboid-like shape (corresponding to a state of reactive microglia) to a more ramified one (as found in unlesioned conditions).

A quantitative analysis of the distribution of microglia cells in different morphological shapes (Figure 3d–e) corroborates the above results: in the naïve group, ON lesion caused an increase of the proportion of ameboid cells, concurrently with a decrease of the ramified ones. In the unlesioned groups, ivt injection per se, independently from the injected solution, decreased significantly the ramified cells and enhanced the rounded Iba1+ cells, compared with the unlesioned naïve, whereas no differences were found in the proportion of ameboid Iba1+ cells (Figure 3e). In PBS- and hNGFwt-treated lesioned retinae, ramified Iba1+ cell number further decreased, whereas the proportion of ameboid microglia cells increased, becoming the most abundant microglial subpopulation in the PBS- and hNGFwt-treated lesioned groups. hNGFp treatment fully rescued the proportion of ramified Iba1+ cells to control values, suggesting that it exerts its neuroprotective effect by shifting the morphological distribution towards more ramified homeostatic microglia (Figure 3e).

In line with these data, both ON lesion and ivt injections markedly boosted the number of CD68+Iba1+ cells, compared with the unlesioned naïve samples (Figure 3f–g). PBS or hNGFwt ivt injections did not further affect CD68 expression from lesioned retinae, whereas hNGFp lowered the number of activated CD68+Iba1+ cells to control values (Figure 3f–g). Altogether, these results pinpoint hNGFp as a molecule able to steer retinal microglia towards a more ramified homeostatic phenotype.

FIGURE 3 hNGFp steers retinal microglia towards a more ramified homeostatic phenotype. (a–c) Graphical representation of parameters used for the analysis of the changes in microglial morphology. Comparison of the area, circularity, A/TI between unlesioned and lesioned naïve animals or after ivt injection of vehicle (PBS), hNGFwt or hNGFp at the dose 1.5 μg/mL. Only hNGFp treatment rescued all the affected parameters to control values (n = 6–7/group, P < 0.05). (d) Confocal image representing three different subpopulations of Iba1+ cells in a neonatal retina. Iba1 immunofluorescence staining in a control PBS-treated retina at P2. The image clearly shows the presence of three different Iba1+ subpopulations: more ramified (microglia; purple arrows), more ameboid (presumably reactive microglia; red arrows) and more rounded (with a faint Iba1 labelling, presumably monocytes; white arrows). Scale bar: 25 μm. (d'–d'') High-power views of cells. (e) Quantitative analysis of the three different subpopulations of Iba1+ cells. Histogram data indicating the percentage of ramified (grey columns), ameboid (white columns) and rounded (chessed columns) Iba1+ cells in unlesioned or lesioned retinae, from P2 naïve pups (no ivt), pups treated by intravitreal injection (ivt) with vehicle (PBS), hNGFwt or hNGFp at the dose of 1.5 μg/mL (n = 6–7/group). Two-way ANOVA, Tukey's multiple comparisons test; *P < 0.05 (for ramified Iba1+ cells). #P < 0.05 (for ameboid Iba1+ cells). §P < 0.05 (for rounded Iba1+ cells). Where not specified, statistical comparisons among groups resulted not significantly different. (f–g) At 1.5-μg/mL dose, only hNGFp decreased CD68+ iba1+ cells following ON lesion. (f) Confocal merge images from unlesioned and lesioned retinae with CD68 (red) and Iba1 (green) co-labelling. Scale bar: 25 μm. (g) Histograms represented CD68+(Iba1+) cell counts in unlesioned (control, white) or lesioned (black) retinae from P2 naïve pups (no ivt), pups treated by intravitreal injection (ivt) of PBS (vehicle), hNGFwt or hNGFp at the dose of 1.5 μg/mL (n = 6–7/group). Optic nerve lesion markedly increased CD68+(Iba1+) cells in naïve retinae. Similarly, in the unlesioned, ivt injection per se significantly enhanced CD68+(Iba1+) cells, whereas PBS- and hNGFwt-treated lesioned retinae showed a comparable Iba1+ cell amount to their respective controls. hNGFp treatment reduced significantly the number of microglial cells expressing CD68 number in lesioned retinae. Two-way ANOVA, Tukey's multiple comparisons test; *P < 0.05; Mean ± standard error.
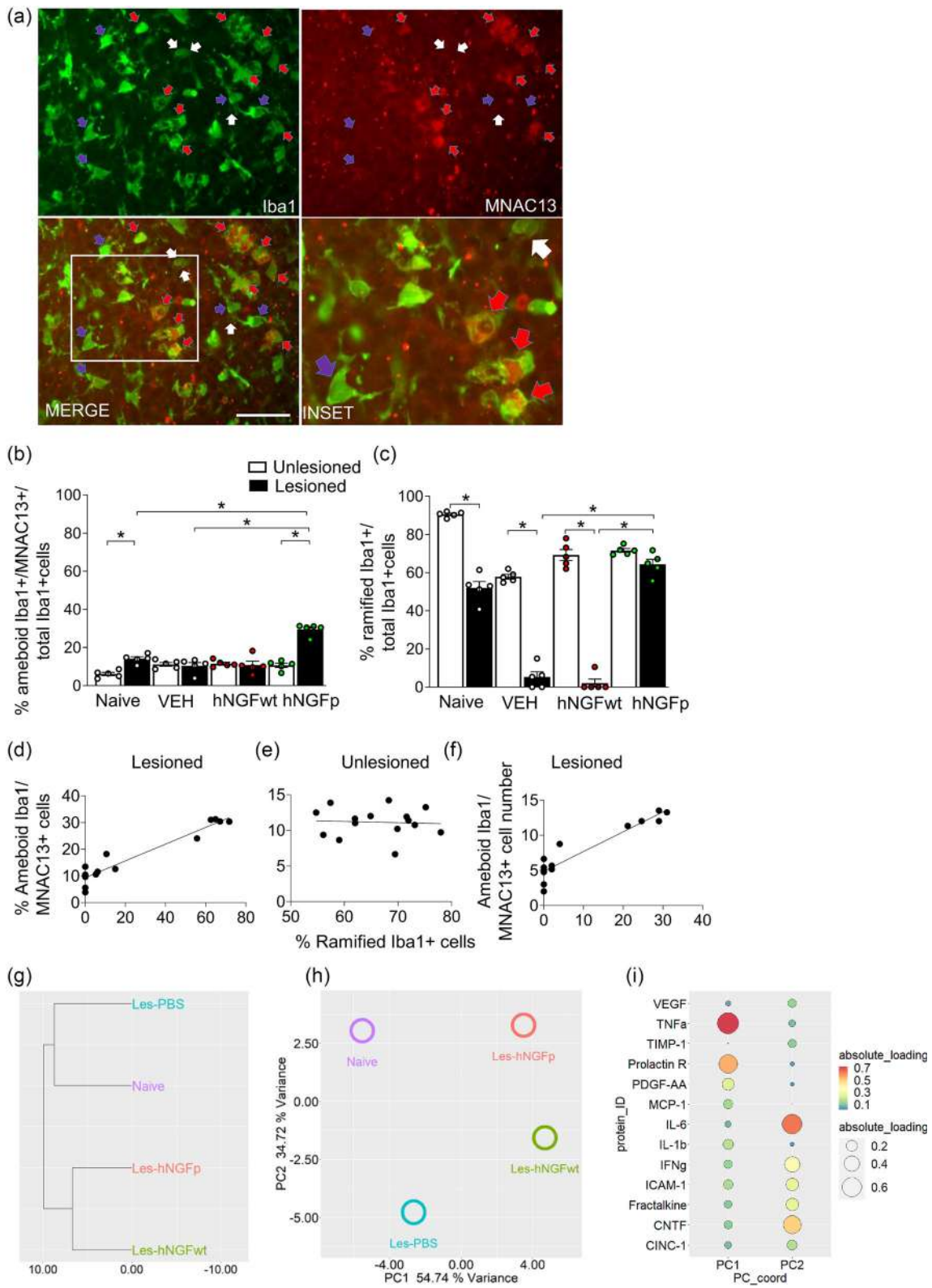
FIGURE 4 Legend on next page.

3.3 | TrkA receptor is selectively expressed by a disease-relevant subpopulation of microglia in neonatal retinae

The above results propose microglia as a new target cell for NGF in the retina, as previously found in the brain, since its high-affinity receptor, TrkA, is expressed in these cells. Given the plethora of morphologies displayed by microglial cells (Savage et al., 2019), it was of interest to examine the expression of TrkA in microglia subpopulations displaying different morphologies in the neonatal retina. As shown in Figure 4a (red arrows), TrkA was observed only in ameboid Iba1+ cells, whereas it was absent in both ramified and rounded cells. We therefore suggest ameboid Iba1+ subpopulation of retinal microglia cells act as a direct target of hNGF pharmacological actions in lesioned retina. In axotomized naive retinae, the percentage of ameboid TrkA-expressing Iba1+ cells significantly increased when compared with the unlesioned samples (Figure 4b). In hNGFp-treated lesioned animals, the percentage of ameboid TrkA+ microglia (MNAC13+/Iba1+) hugely increased (Figure 4b), whereas that of total ameboid microglia significantly decreased compared with PBS- and hNGFwt-injected rats (Figure 3e). This indicates that the low percentage of ameboid microglia found in hNGFp-treated axotomized retinae (Figure 3e) selectively expresses TrkA receptor. In parallel, in lesioned retinae, we observed a huge increase of the proportion of ramified microglia, relative to the ameboid, after hNGFp treatment, in comparison with PBS- and hNGFwt-treated retinae (Figure 4c).

Given these results, we hypothesized that the amount of TrkA+ ameboid microglia might be correlated to that of ramified microglia in lesioned retinae. Correlation analysis revealed that a strong correlation between the percentage of TrkA+ ameboid microglia is strongly correlated with that of ramified cells in lesioned retinae

(Figure 4d). In the uninjured retinae, this relationship was absent (Figure 4e). The positive correlation between TrkA+ ameboid microglia and ramified cells subsisted when overall data from all fields of acquisition from lesioned retinae were pooled (Figure 4f), suggesting that a general hNGFP mechanism operates throughout the whole retina.

Altogether, these data suggest that the lesion enhanced the appearance of the ameboid microglia subpopulation that is TrkA+. hNGFp but not hNGFwt treatments selectively upregulate the percentage of TrkA+ ameboid microglia and this, in turn, leads to a massive increase in the homeostatic ramified microglia. This disease-relevant TrkA+ microglia subpopulation offers a therapeutic opportunity to be pharmacologically targeted by hNGFp.

3.4 | hNGFp rescues more efficiently than hNGFwt the expression of cytokines modulated by the optic nerve lesion and intravitreal injection

To further link the observed changes of cellular morphology to the phenotype and functional state of microglia, we profiled a panel of 26 cytokines and chemokines in naïve and lesioned retinae from rat pups after ivt injections of PBS, hNGFwt or hNGFp (1.5 μg/mL). Hierarchical clustering demonstrated that hNGFwt and hNGFp have a similar cytokine profile, although in the Euclidean distance matrix, on which clustering is based, hNGFp is closer to naïve than hNGFwt (Figure 4g). Principal component analysis also confirms that hNGFp is closer to naïve than hNGFwt (Figure 4h). This likeness was predominantly determined by TNFα and prolactin R, the proteins with the largest projections (loadings) on PC1 (Figure 4i). Hence, at this tested dose, hNGFp was superior to hNGFwt in reverting cytokine levels modulated by the lesion and the ivt injection.

FIGURE 4 TrkA receptor is selectively expressed in ameboid Iba1+ cells. (a) Confocal images from a neonatal retina with Iba1 (microglia/macrophages marker) and MNAC13 (TrkA marker) immunolabelling. Differently from ramified (purple arrows) or rounded (white arrows) Iba1+ cells, only ameboid Iba1+ cells (red arrows) expressed the TrkA receptor. Scale bar: 25 μm. (b–c) Quantitative analysis of the ameboid TrkA-expressing Iba1+ microglia and ramified Iba1 cells. (b) Histogram data of the percentage of ameboid Iba1+/MNAC13+ (TrkA marker) cells, in unlesioned (white bars) or lesioned (black bars) retinae from naïve P2 pups (no intravitreal injection) or pups treated by ivt with vehicle (PBS), hNGFwt or hNGFp at the dose of 1.5 μg/mL (n = 5/group). (c) Percentage of ramified microglia in different experimental conditions as reported in B. Two-way ANOVA, Tukey's multiple comparisons test *P < 0.05. Mean ± standard error. (d–e) Ameboid TrkA+ and ramified microglia were strictly correlated. Scatterplots showing the relationship between the percentage of ameboid Iba1+/MNAC13+ cells versus ramified Iba1+ cells from lesioned (d; r = 0.957, P < 0.05) and unlesioned (e; r = −0.063, P = 0.825) retinae of mice treated by ivt injection with vehicle (PBS), hNGFwt or hNGFp at the dose of 1.5 μg/mL (n = 5/group). Pearson correlation's coefficient was used for correlation analysis. Each point represents an average of eight fields of acquisition from each retina (same equivalent fields in different retinas), from the different experimental conditions. (f) Same as in (d) and (e), but displaying the relationship between the number of ameboid TrkA+ microglia cells and the fraction of ramified cells on total microglia (r = 0.868, P < 0.05). (g–i) hNGFp rescues more efficiently than hNGFwt the expression of candidate cytokines involved in the optic nerve lesion and intravitreal injection of neonate rats. Whole retina homogenates were probed by cytokine array and the group average is shown. (g) Hierarchical clustering of group averages demonstrates that naïve and lesioned intravitreally injected retinae have similar global cytokine profiles, distinct from the NGF-treated ones. (h) Principal component (PC) analysis, in which PC1 and PC2 are the first two principal components with the proportion of variance represented by these components: hNGFp-treated lesioned retinae (Les-hNGFp) are closer to naïve retinae than hNGFwt-treated lesioned (Les-hNGFwt) and are further from PBS-treated lesioned retina (Les-PBS) than Les-hNGFwt. (i) The PCA loading plot (absolute values) shows that this separation was predominantly driven by the contribution of TNFα and prolactin R (PC1) and IL-6 and CNTF (PC2). The circle size is proportional to loading value, corresponding also to the colour scale.
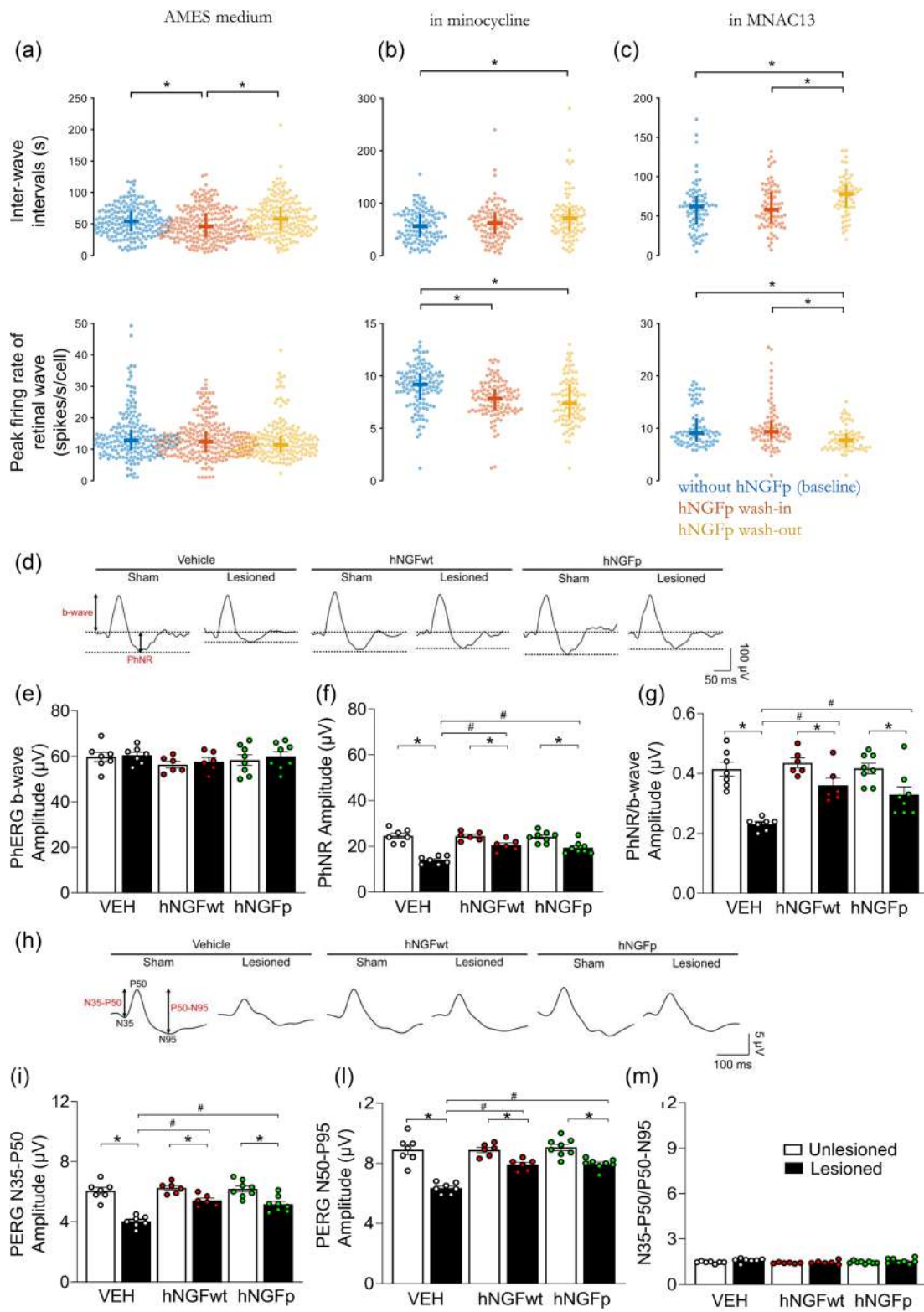
FIGURE 5 Legend on next page.

3.5 | hNGFp modulates electrical retinal activity in neonate and adult rodents

To gain direct evidence on the functional consequences of the hNGFp-mediated neuroprotection of RGC and on the possible involvement of TrkA-expressing microglia, MEA recordings of spontaneous RGC activity were performed from neonatal unlesioned rat retinae. Specifically, we examined the characteristics of retinal waves, that is, the spontaneous travelling waves of correlated spike bursts among RGCs (Figure 5).

Bath application of hNGFp significantly decreased IWIs (Figure 5a, top)—that is, increased the frequency of retinal waves—without affecting the peak firing rate (Figure 5a, bottom). Conversely, by blocking microglia activation with minocycline administration (100 nM), no significant changes in IWIs were induced by hNGFp (Figure 5b, top). This suggests that hNGFp facilitates retinal waves by acting on microglial cells. The microglial inhibitor *per se* increased IWIs over time (Figure 5b, top) and decreased the peak firing rate (bottom), indicating a microglial tonic control of retinal waves. Consistent with this observation, in the presence of the neutralizing anti-TrkA mAb MNAC13 (1 μg/mL), hNGFp had no significant effect on IWIs (Figure 5c, top). Furthermore, like minocycline, MNAC13 *per se* increased IWIs over time (Figure 5c, top) and decreased the peak firing rate (Figure 5c, bottom). These results support a TrkA-mediated microglial control of spontaneous RGC activities in the mouse neonatal retina by endogenous NGF levels.

The functional effects of NGF-based drugs and vehicle on RGC-dependent visual responses were investigated in adult rats, by measuring the cone-driven photopic electroretinogram (phERG) 17 days after ONC and after 13 days of treatment, started at day 4 post-surgery.

In adult rats, ONC did not affect the phERG b-wave component (Figure 5e), which arises from the post-cone-receptor activity, whereas it produced a significant reduction of the amplitude of the photopic negative response (phNR) component, arising from the RGC activity (Figure 5f).

In unlesioned adult rats, neither hNGFwt nor hNGFp affected the PhNR and b-wave components of the phERG response, as compared with the vehicle-treated group (Figure 5d–f, empty bars). As expected, the vehicle-treated ONC group displayed a reduction of the PhNR amplitude of about 44%, in relation to the vehicle-treated sham (Figure 5d–f, black bars). In ONC rats, either hNGFp or hNGFwt treatment rescued by 48% the reduced PhNR amplitude observed in vehicle-treated ONC animals (Figure 5d–f).

To exclude the contribution of the outer retinal activity in the NGF modulation of the PhNR, the individual PhNR/b-wave component, in the context of each individual phERG response, was analysed in the various groups (Figure 5g). The deriving outcomes overlapped with the non-normalized PhNR results (Figure 5f), pointing to a direct effect of NGF on RGC activity that is unrelated to variations in the outer retinal activity.

Subsequently, we investigated the activity of RGCs with pattern-ERG (PERG). We observed a significant reduction of the amplitudes of the PERG N35-P50 and P50-N95 components in the vehicle-treated lesioned rats compared with the vehicle-treated sham group, which was partially recovered by hNGFp or hNGFwt (Figure 5h–l). Both hNGFp or hNGFwt treatment, in lesioned or sham groups, influenced the PERG components proportionally, as highlighted by the ratios of

FIGURE 5 hNGFp modulates electrical retinal activity in neonate and adult rats. (a) hNGFp increased the frequency of retinal waves without affecting their peak firing rate. Retinal waves, that is, the spontaneous travelling waves of correlated spike bursts among RGCs, are defined as events with an average population firing rate above a threshold of 1 spike per second per cell. Top: inter-wave intervals before (n = 191 cells; blue), during (n = 229 cells; orange) and after (n = 187 cells; yellow) hNGFp application (54 ± 17 s, 46 ± 18 s, 58 ± 19 s, respectively). Bottom: Peak firing rate of the retinal waves for the same dataset as in the top (in spikes/s/cell for the three conditions: 12.8 ± 3.2, 12.4 ± 3.3, 11.4 ± 2.6). Median ± median absolute deviation marked in bold horizontal and vertical lines, respectively; n = 10 retinae. (b) Blocking microglial cell activation attenuates hNGFp effect. (a) Inter-wave intervals in the continuous presence of the microglia activation blocker minocycline (100 nM) before (n = 115 cells), during (n = 106 cells) and after (n = 85 cells) hNGFp application (56 ± 23 s, 62 ± 20 s, 71 ± 21 s, respectively; mean ± standard deviation marked in bold horizontal and vertical lines, respectively; n = 6 retinae). Bottom: Peak firing rate of the retinal waves for the same dataset as in the Top (in spikes/s/cell for the three conditions: 9.2 ± 1.1, 7.8 ± 1.1, 7.4 ± 1.4). (c) Blocking TkA receptor attenuates hNGFp effect. Top: Inter-wave intervals in the continuous presence of anti-TrkA antibody (1 mg/mL MNAC13) before (n = 75 cells), during (n = 73 cells) and after (n = 60 cells) hNGFp application (62 ± 16 s, 58 ± 21 s, 78 ± 16 s, respectively; mean ± standard deviation marked in bold horizontal and vertical lines, respectively; n = 4 retinae). Bottom: Peak firing rate of the retinal waves for the same dataset as in the Top (in spikes/s/cell for the three conditions: 9.1 ± 1.8, 9.3 ± 1.6, 7.7 ± 1.4). One-way Kruskal–Wallis ANOVA with Dunn's post hoc test: *$P < 0.05$. (d) Representative waveform displaying phERG b-wave, arising from the cone-driven post-receptoral activity, and PhNR, arising from RGC activity, from either sham or ON lesioned rats treated with 25 μL of vehicle, hNGFp (200 μg/mL) or hNGFwt (200 μg/mL) instilled three times per day. (e–f) Quantification of phERG b-wave (e) and PhNR (f) amplitudes. (g) Individual PhNR/phERG b-wave amplitude ratios as a quantitative RGC-related output corrected for the outer retinal contribution. (h) Representative waveform displaying PERG N35-P50 and P50-N95 amplitudes from either sham or ON lesioned rats treated with 25 μL of vehicle, hNGFp (200 μg/mL) or hNGFwt (200 μg/mL) instilled three times per day. Quantification of PERG N35-P50 (i) and P50-N95 (l) amplitudes. (m) Individual N35-P50/P50-N95 amplitude ratios to ascertain the proportionality of PERG components modulation among experimental groups. Data are reported as mean ± SEM [vehicle sham (n = 7), vehicle lesioned (n = 7), hNGFwt sham (n = 8), hNGFwt lesioned (n = 8), hNGFp sham (n = 6) and hNGFwt lesioned (n = 6)]. Differences among groups were tested using two-way ANOVA, followed by Tukey's multiple comparisons test. *$P < 0.05$ sham versus lesioned and #$P < 0.05$ lesioned versus hNGFwt/hNGFp lesioned.
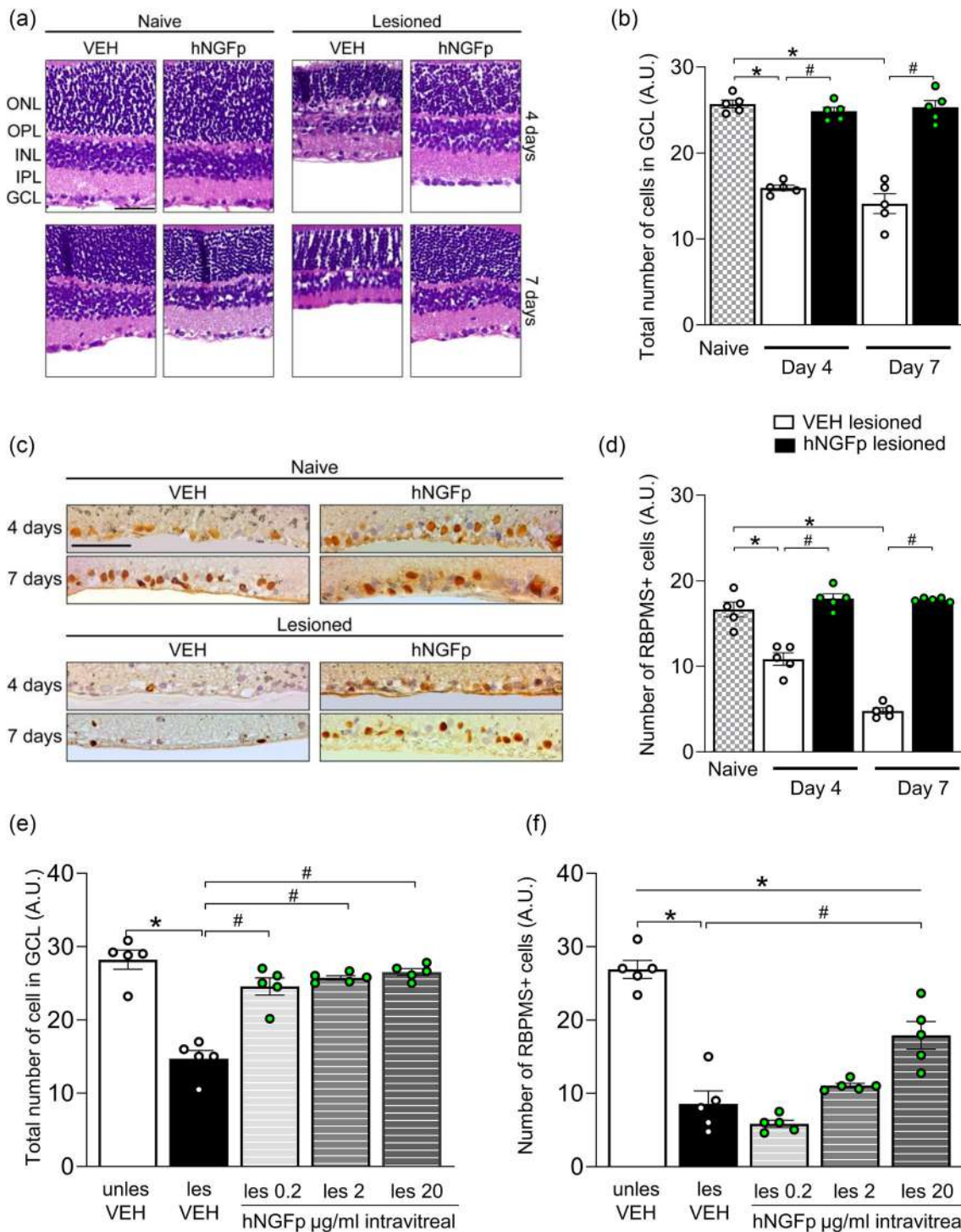
FIGURE 6 Intravitreal injections of hNGFp rescue cells in the GCL of adult rat retina. (a) Light micrographs, haematoxylin and eosin stain of retinal sections from adult rats with unlesioned and lesioned ON, receiving daily intravitreal injections of 2-μL vehicle (PBS) or hNGFp (2 μg/mL) for 4 or 7 days immediately after the lesion. (b) Histogram of the total cell number in ganglion cell layer (GCL) from naïve retinae and PBS or hNGFp-treated retinae at day 4 and 7 after ON lesioned. (c) RGC (RBPMS) immunohistochemistry staining of retina sections from naïve and lesioned rats, treated with PBS or hNGFp as in (a). (d) Histogram of the number of RGC (RBPMS+ cells) from naïve retinae and PBS or hNGFp-treated retinae at day 4 and 7 after ON lesioned. (e) Histogram of the total cell number in GCL from unlesioned and lesioned retinae ivt injected with PBS and lesioned hNGFp-treated retinae (0.2, 2 and 20 μg/mL intravitreal injection 2 μL, every day, immediately after ON lesion, for 7 days. (f) Histogram of the number of RBPMS+ cells in GCL from retinae injected with vehicle or different hNGFp doses, starting at day 4 after injury and lasting until day 7. Data are mean ± SEM, n = 5 rats for each experimental condition; two-way ANOVA, Tukey's or multiple comparisons test. *$P < 0.05$ naïve versus lesioned or unlesioned vehicle versus lesioned vehicle (e–f); #$P < 0.05$ PBS lesioned versus hNGFp lesioned, §$P < 0.05$. Scale bar: 50 μm. GCL, ganglion cell layer; IPL, inner plexiform layer; INL, inner nuclear layer; OPL outer plexiform layer; ONL, outer nuclear layer.
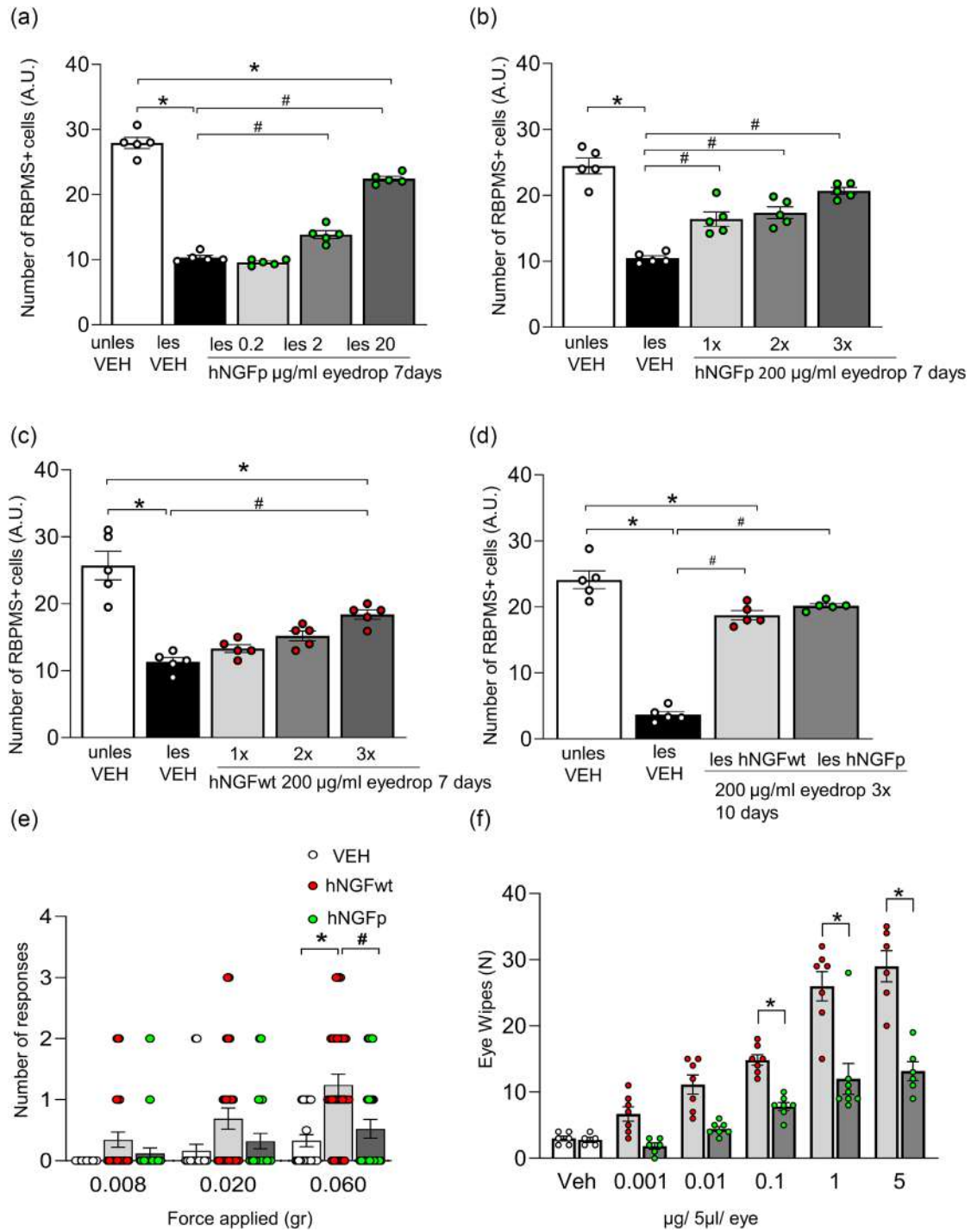
FIGURE 7   Legend on next page.

the N35-P50/P50-N95 amplitudes, resulting in statistically comparable ratios among groups (Figure 5m). Finally, to exclude any effects of the outer retina on the modulation of RGC activity by the lesion as well as by hNGFp and hNGFwt treatment, we analysed the amplitudes of the scERG a-wave, arising from the overall rod photoreceptor activity and of the scERG b-wave, arising from the activity of bipolar, amacrine and Müller cells. As shown in Figure S1, the amplitude of both components of the scERG was not affected by the ONC, nor by pharmacological treatments as compared with the respective control groups.

Altogether, these data indicate that adult rat ON lesion induces a drastic decrement of RGC activity without altering the outer retinal function, by damaging the ganglion cell bodies and nearby structures, the ON (N35-P50) and the action potential conduction along axons and ON (P50-N95) (Winn et al., 2005). As for the outcome of hNGFp and hNGFwt treatments, they restore electrophysiological parameters by counteracting the lesion-driven damage of RGC bodies and axons, at both central and peripheral retina areas, without acting on outer retinal function.

3.6 | Intravitreal and eye drop hNGFp rescues RGC degeneration in an adult rat model of retinal degeneration

Having established that eye drop delivery of hNGFp to adult rats restores RGC-dependent electrophysiological functions, we tested whether hNGFp or hNGFwt eye drop formulations might rescue RGC degeneration in adult rats. First, we confirmed the neuroprotective effects of ivt injection hNGFp in adult rats, as we found in the neonatal retina (Figure 1). Immediately after ONC, both eyes of the same animal (left eye: lesion; right eye: control) received an ivt injection (2 μL) of either PBS or hNGFp.

In vehicle-treated retinae, ONC significantly decreased the number of GCL cells and of RGC, assessed at days 4 and 7 after injury, relative to unlesioned retinae (Figure 6a–d). Compared with the total number of cells in GCL (amacrine cells, RGC, microglia and astrocytes; Figure 6b), which is equally reduced at day 4 and day 7, the RBPMS+ cell reduction was time-dependent in lesioned retinae, with a higher

cell loss 1 week following ONC (Figure 6d). Administration of 2-μL ivt hNGFp (2 μg/mL), each day following nerve injury, fully counteracted the reduction of both total cells and RGCs in the GCL (Figure 6a–d).

Further dose-dependent experiments revealed that hNGFp, administered for 7 days starting immediately after the ONC, was already effective in reducing the decreased cell number in GCL at the concentration of 0.2 μg/mL, as well as at other higher doses tested (2 and 20 μg/mL; Figure 6e).

Altogether, these results show that ivt injected hNGFp prevents the reduction of cells caused by ONC in GCL of adult rats.

We then carried out experiments to assess the therapeutic efficacy of hNGFp, delivered ivt after ONC. On the fourth day from the nerve injury, hNGFp was ivt administered for 4 days at different doses (Figure S2). Compared with vehicle-treated lesioned retinae, hNGFp ivt administration, at the concentration of 20 μg/mL, increased the total number of survived cells in the GCL and of RGCs, whereas at lower doses tested (0.2 and 2 μg/mL), it resulted ineffective (Figure S2A for GCL cells and Figure 6F for RGCs). These data demonstrate that the dose of 20-μg/mL hNGFp, administered 4 days after the establishment of the retinal neurodegeneration, effectively counteracts the loss of cells in the GCL.

In a clinical perspective, in view of a better compliance of patients, a non-invasive eye drop formulation would be desirable. Building on these results, we next evaluated the efficacy of the non-invasive hNGFp-based eye drop treatment. Eye drops containing hNGFp 2 or 20 μg/mL, 1 week daily administered, starting immediately after ONC, significantly increased the amount of RBPMS+ cells in lesioned retinae as compared with vehicle-treated retinae (Figure 7a). The total number of surviving cells in the GCL was significantly higher in the retinae from injured rats treated with 20-μg/mL hNGFp than those receiving vehicle containing eye drops (Figure S2B).

Eye drop treatment with a higher dose of hNGFp (200 μg/mL), daily administered once, twice or thrice, starting on the fourth day after ONC until day seven, significantly increased the number of survived RBPMS+ cells (Figure 7b), whereas only hNGFp administered 3 times enhanced the total number of surviving cells in the GCL (Figure S2C).

Subsequent head-to-head comparison experiments showed that hNGFwt at the same dosing regimen provided RGC neuroprotection

FIGURE 7 hNGFp eye drop treatment is more effective than hNGFwt in reverting RGC death. (a) Cumulative data expressed as number of RBPMS+ cells in the GCL at day 7 after ON lesion after hNGFp (0.2, 2 and 20 μg/mL eye drop 25 μL, every day for 7 days) treatment. (b) histogram of number RBPMS+ cells in the GCL from unlesioned and lesioned retinae from rats receiving PBS or hNGFp-based eye drops on the fourth day from ON lesion for 7-day treatment [200 μg/mL eye drop 25 μL, once (1×), twice (2×) and three (3×) times a day]. (c) Same as in (b) but with hNGFwt-based eye drops. Note that hNGFp is more effective than hNGFwt. (d) Histogram of the total number of RBPMS+ cells from unlesioned and lesioned retinae on the 14th day after ON lesion and following a 10-day treatment with PBS or hNGFp or hNGFwt at 200-μg/mL eye drop 25-μL doses. Note that at higher dose, the number of RGC in hNGFp-treated lesioned retinae is similar to the unlesioned, whereas in hNGFwt is not (n = 5). (e) Histogram of the total head retractions (number of response) upon different von Frey filament force applications, in three different experimental group: animals treated with vehicle (bidistilled water; n = 25; empty circle), animals treated with hNGFp (n = 25; green circle) and animals treated with hNGFwt (n = 29; red circle). (f) Dose-dependent eye wiping response evoked by ocular instillation (5 μL/drop eye) of vehicle (empty circle), hNGFwt (red circle) and hNGFp (green circle; 0.001–5 μg) in C57BL/6 mice. Data are mean ± SEM, n = 5–8 mice for each experimental condition. One-way ANOVA, Tukey's multiple comparisons test, * $P < 0.05$, unlesioned versus lesioned; #$P < 0.05$, PBS lesioned versus hNGFwt/hNGFp lesioned. In (e), # vehicle versus hNGFwt, * hNGFwt versus hNGFp.

only if administered three times and not when administered once or twice (Figure 7c, in comparison with Figure 7b with hNGFp). When we looked at the total cells in GCL, hNGFwt-based eye drops, administered two or three times daily, rescued the total number of cells in GCL from ON lesioned rats (P < 0.001 hNGFwt lesioned vs. PBS lesioned; Figure S2D). Altogether, these data show that hNGFp eye drops are more effective than hNGFwt in rescuing RGC survival following ONC, whereas the effect of hNGFp and hNGFwt for GCL cells is comparable.

Since RGC loss is abrupt and occurs during the first 2 weeks after ON injury (Villegas-Pérez et al., 1993), we evaluated the therapeutic effectiveness of hNGFp or of hNGFwt on the 14th day after lesion, following 10 days of daily eye drop treatment, starting on the fourth day after nerve crush. As shown in Figure 7d, the very large RGC loss observed 14 days after nerve injury was significantly rescued by both hNGFp- and hNGFwt-based eye drops. Notably, only hNGFp treatment fully rescued RGCs, being the amount of RGCs in hNGFp axotomized retinae was similar to the unlesioned samples. The residual number of survived cells in GCL following ON injury was significantly reversed near to control numbers by both hNGFp and hNGFwt (Figure S2E).

In unlesioned retinae from adult rats, hNGFp ivt injections and eye drops at different doses did not affect the RGC number and more generally cells in the GCL (Figure S3A–D,G). In contrast, hNGFwt induce a small but significant decrease of the RGC number in unlesioned rats (Figure S3F).

Overall, at lower doses hNGFp more efficiently counteracted RGC death than hNGFwt and presented a safer profile than its native neurotrophin counterpart.

3.7 | hNGFp-based ocular drops do not induce eye pain sensitization

In patients, ocular administration of hNGFwt induces eye pain due to the intrinsic property of this neurotrophin to regulate nociceptive signalling (Bonini et al., 2018; Lewin et al., 1993; Li et al., 2023; Pflugfelder et al., 2020). The algogenic activity is significantly reduced by hNGFp compared with hNGFwt when injected in the paw for mechanical allodynia and thermal pain evaluation, as well as when delivered nasally for orofacial pain evaluation (Capsoni et al., 2017; Malerba et al., 2015). However, the potential ocular or oro-facial pain elicited by hNGFp eye drops has never been tested. We therefore performed the von Frey filament test to assess the hypersensitivity to mechanical stimulation of the trigeminal area innervating the eye, before and following 1-week-daily administration of eye drops containing vehicle, hNGFwt or hNGFp. We found that although hNGFwt-treated mice showed a significantly higher number of head retractions in response to 0.06 g force application, mice receiving hNGFp did not show increased head withdrawal at all forces applied (Figure 7e). Moreover, when mice received on the ocular surface 5 μL of different concentrations of hNGFp or hNGFwt eyedrops (0.001,0.01, 0.1, 1 and 5 μg/5 μL), the latter induced a higher number

of eye-wipes at all doses tested, compared with those elicited by hNGFp (Figure 7f). Altogether, these results show that, unlike hNGFwt, hNGFp-based ocular drops do not induce eye pain sensitization or irritation.

3.8 | hNGFp increases the expression of GAP-43 in the lesioned axonal stump

RGC degeneration was associated with a decrease of the axonal growth marker, GAP-43 (Holahan, 2017), beyond the crush site (Figure S4A). In parallel to a recovery of the number of RGC (Figure 7b), 4-day eye drop treatment with 200-μg/mL hNGFp, starting at day 4 after ON injury, significantly increased the expression of GAP-43 in the injured nerve trunk (Figure S4B-E). In particular, one, two or three times a day of hNGFp eye drops significantly increased the number of GAP-43$^+$ axons, at a distance of 0.25 μm from the crush site. At longer distance from the ON injury (around 100–200 μm), the number of GAP-43-positive axon stumps was increased by hNGFp, even if only at the 2× and 3× daily dosing doses (P < 0.05, hNGFp lesioned vs. veh lesioned; Figure S4E).

A prolonged eye drop treatment (10 days) with hNGFp or hNGFwt was more effective in raising GAP-43+ axon number, at each distance point and for farther distances from the lesion (Figure S4F-I).

These results show that the neuroprotective and anti-neurodegenerative effects of hNGFp shown above are associated with the increased expression of the axonal growth marker GAP-43. It remains to be seen whether the increased expression of GAP-43 might be associated with a more general activation of a global axon-growth gene expression program.

3.9 | hNGFp rescued reactive microglia in lesioned adult retinae

Following ON damage, microglial cells respond by adopting a reactive phenotype, likely contributing to the retinal degeneration (Garcia-Valenzuela et al., 2005; Thanos et al., 1993). Similarly to the microgliosis detected in neonatal lesioned retinae (Figure 2c–d), ON crush increased significantly the microglia density at both days 4 and 7 in retinae from adult rats (for both days 4 and 7; Figure 8a–b) as well as the number of Iba1$^+$OX6$^+$ microglial cells at day 7 after the nerve crush (Figure 8e–f).

The administration of 200-μg/mL hNGFp eye drop, delivered twice or three times a day for 4 days from day 4 after ONC, effectively reduced the enhanced density of Iba1$^+$ cells (Figure 8c–d) and of the activated Iba1$^+$OX6$^+$ microglial cells (Figure 8e–f).

We then compared the hNGFp effectiveness relative with that of hNGFwt on the 14th day from ON lesion, after their topical application three times a day for 10 days. We found that upon this dosage and administration schedule, both drugs lowered the increased density of microglia and their reactive phenotype in lesioned retinae (Figure S5A–C).
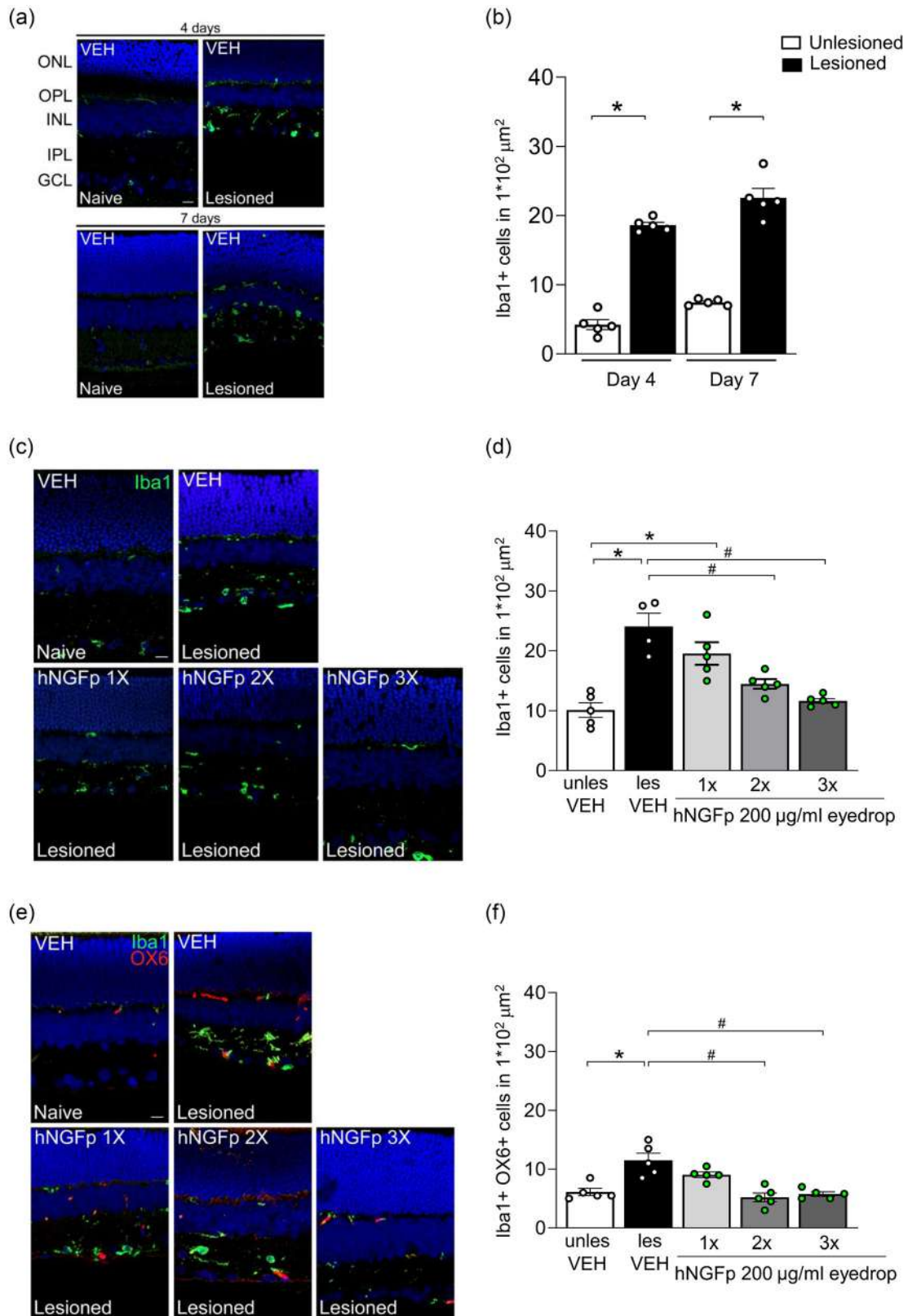
FIGURE 8 Legend on next page.

To further investigate the phenotype of reactive microglia in adult rat lesioned retinae, we carried out immunofluorescence assays on the proinflammatory cytokines IL-1β, IL-6 and TNFα. With respect to vehicle-treated unlesioned (naïve) retinae, the intensity of IL-1β, IL-6 and TNFα immunofluorescence staining significantly increased in lesioned retinae, spreading from the GCL in control tissues to the IPL and INL in lesioned retinae (Figure S6A–C). This enhanced fluorescence signal was abolished in retinae from lesioned rats receiving 10-day hNGFp eye drops treatment (Figure S6A–D). In head-to-head experiments, retinae from animals receiving hNGFwt at this dosage regimen exhibited a substantially reduced cytokine immunofluorescence signal in relation to vehicle-treated retinae (Figure S6A,E–G).

3.10 | hNGFp ocular drops pharmacokinetics in rabbits

The remarkable neuroprotective effectiveness of hNGFp in reverting RGC neurodegeneration is of high clinical relevance. As a further step towards clinical advancement, a pharmacokinetic study after hNGFp eye drops was performed in rabbits, since they have similar eye size to humans, and a large database of information for comparison favours performing pharmacokinetic studies using rabbit eyes. Mean hNGFp concentrations in plasma, retina and vitreous humour samples collected 24 h after a 14-day ocular topical administration of three different dose regimens (100, 200 and 400 μg/day) in adult rabbits are shown in Table 2. The main result of this PK study is that, after eye drop delivery, biologically relevant quantities of hNGFp are found in the rabbit's retina. Mean hNGFp concentrations in the retina were higher than those measured in the plasma and in the vitreous humour.

4 | DISCUSSION

In this study, we analysed the neuroprotective properties of intravitreal and eye drop hNGFp on rat RGC degeneration following ON lesion in comparison with the neuroprotective properties of hNGFwt. We found that hNGFp displays remarkable neuroprotection in a therapeutic experimental setting and that this action is mediated mainly by TrkA-positive retinal microglial cells.

Moreover, in various experimental paradigms, hNGFp displayed superior properties compared with hNGFwt, in that at lower doses the actions of the two proteins could be differentiated, in reducing RGC loss and in modulating levels of different cytokines. Furthermore,

hNGFp did not impact on the number of healthy RGCs in unlesioned retinae from adult rats, whereas hNGFwt decreased the RGC number. In a few experiments, in which we observed no distinction between hNGFp and hNGFwt efficacy, it may be surmised that the doses of hNGFwt were already considerably high and that neurotrophic TrkA-derived signalling is able to overcome the negative consequences of that of p75NTR. Finally, we showed that ocular pain threshold is higher in animals receiving hNGFp eye drops than in mice treated with hNGFwt, allowing treatments with higher doses and possibly improving patient compliance in future clinical trials.

Altogether, the results demonstrate that hNGF-based drugs have a high therapeutic potential to counteract the loss of RGC that occurs in several ocular diseases. The results also show that hNGFp has a broader therapeutic window than hNGFwt. The superior efficacy and safety of hNGFp rely on its selective binding to TrkA, with a reduced affinity to p75NTR compared with hNGFwt, thus behaving as a TrkA-biased and p75NTR-sparing agonist (Covaceuszach et al., 2010). It is noteworthy that in previous studies, NGF failed to rescue axotomized RGCs, whereas a selective TrkA agonist, or NGF plus a p75NTR antagonist, produced a substantial neuroprotection (Bai et al., 2010; Lebrun-Julien et al., 2009; Shi et al., 2007).

Consistently, when the two NGF receptors are co-expressed in the same cell, p75NTR enhances the affinity and selectivity of TrkA receptors for NGF, whereas it induces apoptosis and cell death in response to its activation (Frade et al., 1996; Lee et al., 2001). In oligodendrocytes that experience NGF-dependent apoptosis via p75NTR, TrkA receptor activation by NGF negates cell death (Yoon et al., 1998). In PC12 cells genetically edited to lack p75NTR, NGF-mediated TrkA effects are enhanced (Testa et al., 2022). Also, the effectiveness of NGF-induced RGC neuroprotection in ON lesioned rodents is doubled in p75NTR$^{-/-}$ mice (Lebrun-Julien et al., 2009). Thus, the overall picture is that the outcome of TrkA and p75NTR activation by NGF is under a competitive equilibrium that is altered in pathological situations, when the expression of p75NTR is greatly elevated (Chao, 2003; Dechant & Barde, 2002; Schoups et al., 1995).

In addition to such cell-autonomous signalling interactions between co-expressed NGF receptors, the outcome of TrkA and p75NTR signalling could also vary when the two receptors are expressed in distinct cell types. In this study, we provide new evidence for a non-cell-autonomous inter-cellular mechanism of hNGFp and hNGFwt in the RGC neuroprotection. So far, the NGF-mediated neuroprotection of RGC degeneration was believed to be ensured exclusively by a direct neurotrophic action on RGCs, even if the expression of TrkA on RGCs is far from being firmly established, at

FIGURE 8 hNGFp rescued reactive microglia in lesioned adult retinae. (a–b) Representative images and cumulative data of Iba1+ cells (in green) in the retina at days 4 and 7 after ON lesion. Microglia density significantly increases following lesion. Data are mean ± SEM of n = 5 rats for each experimental condition. (c–d) Representative images and cumulative data of Iba1$^+$ cells at day 7 after ON lesion, following 4 days of hNGFp eyedrops [200 μg/mL eye drop 25 μL, once (1×), twice (2×) and three (3×) times a day starting at day 4 and lasting until day 7 after lesion]. (e–f) As in (c–d) but with the addition of the activated microglia marker, OX6 (in red). Data are mean ± SEM of n = 5 rats for each experimental condition; one-way ANOVA, Tukey's multiple comparisons test. *P < 0.05 unlesioned versus lesioned and # P < 0.05 lesioned versus hNGFp lesioned. Scale bar: 20 μm. GCL, ganglion cell layer; IPL, inner plexiform layer; INL, inner nuclear layer; OPL outer plexiform layer; ONL, outer nuclear layer.

TABLE 2 hNGFp ocular drops pharmacokinetics in rabbits.

Dose (μg/day)	Gender	Plasma (ng/mL)	Retina (ng/g)	Vitreous Humor (ng/mL)	Dose (μg/day)	Gender	Plasma (ng/mL)	Retina (ng/g)	Vitreous Humor (ng/mL)	Dose (μg/day)	Gender	Plasma (ng/mL)	Retina (ng/g)	Vitreous Humor (ng/mL)
100	Male	0.086	0.140	0.008	200	Male	0.016	0.649	0.031	400	Male	0.005	2.870	0.087
100	Male	0.107	0.127	0.000	200	Male	3.420	0.110	0.044	400	Male	0.005	0.528	0.049
100	Male	0.029	0.472	0.000	200	Male	0.007	0.156	0.068	400	Male	0.044	0.442	0.000
100	Male	0.059			200	Male	0.040			400	Male	0.008		
100	Male	0.009			200	Male	0.014			400	Male	8.790		
100	Female	0.013	0.000	0.018	200	Female	0.045	0.115	0.102	400	Female	0.033	2.820	0.031
100	Female	0.014	0.591	0.021	200	Female	0.006	0.119	0.034	400	Female	0.004	0.175	0.069
100	Female	0.068	0.169	0.000	200	Female	0.247	0.076	0.046	400	Female	0.006	0.402	0.018
100	Female	0.022			200	Female	0.455			400	Female	0.010		
100	Female	0.005			200	Female	0.242			400	Female	0.013		
	n	10	6	6		n	10	6	6		n	10	6	6
	Mean	0.041	0.250	0.008		Mean	0.449	0.204	0.054		Mean	0.892	1.206	0.042
	SD	0.036	0.229	0.010		SD	1.055	0.219	0.027		SD	2.775	1.275	0.033
	SEM	0.011	0.093	0.004		SEM	0.334	0.090	0.011		SEM	0.878	0.520	0.013

Note: Mean (± SEM) hNGFp concentrations in plasma, retina and vitreous humor 24 h after the last administration of 2-week topical ocular application to adult rabbits.

both the protein and mRNA levels (Benhar et al., 2023; Garcia et al., 2017; Lebrun-Julien et al., 2009). Here, we show that, as in the brain (Capsoni et al., 2017; Capsoni & Cattaneo, 2022; Rizzi et al., 2018; Tiberi et al., 2023), hNGFp and hNGFwt predominantly act via retinal microglia, to prevent and rescue neuronal (RGC) death indirectly. This conclusion is founded upon the following findings: (i) in the retina, TrkA receptor is mainly expressed by microglia and not by most RBPMS+ cells. The specificity of the immunostaining by the anti-TrkA mAb MNAC13 is confirmed by the lack of staining in Iba1$^+$ cells from TrkA$^{-/-}$ tissues; (ii) in neonatal retinae, TrkA receptor is uniquely expressed by a selective disease-relevant population of microglia (ameboid Iba1+ cells), whereas it was absent in ramified microglia; (iii) the increased density and morphological changes of retinal microglia, observed following ON lesion, are reversed following hNGFp ocular administration; (iv) the rescue of RGC number correlates with the decrease of microglia cell number in lesioned retinae treated with hNGFp; and (v) inhibiting microglia activation and TrkA receptor signalling abolished hNGFp-mediated RGC wave facilitation. Indeed, our immunofluorescence and electrophysiological results strongly suggest that hNGFp mediates RGC neuroprotection, along with the enhancement of retinal waves, by acting mostly on TrkA$^+$ microglia. However, we cannot exclude an additional direct contribution of hNGFp on RGC.

Given the prominent role of spontaneous RGC activity in the refinement of retinal projections during development (Katz & Shatz, 1996; Maffei & Galli-Resta, 1990), we propose the enhancement of RGC neural activity by hNGFp as a key factor promoting the activation of a neuroprotective and nerve regeneration gene expression program of RGC axons in the ONC model (Lim et al., 2016; Varadarajan et al., 2023).

In line with previous studies (Frade & Barde, 1998), our functional data on neonatal retina clearly suggest that both microglia and TrkA receptor activation by endogenous NGF or by applied hNGFp play a major role in maturation of retinal circuitry. As a whole, the data provide a functional correlation between the TrkA expression on microglia and the final neuroprotective outcome of NGF and hNGFp on RGC. Notably, the resident immune cells of the retina have emerged as an essential cell type critically involved in the onset and progression of RGC degeneration (Margeta et al., 2022; Pan et al., 2023; Silverman & Wong, 2018).

Therefore, we suggest that hNGFp exerts neurotrophic effects on axotomized or lesioned RGCs mainly through microglia. Indeed, hNGFp steers retinal microglia to a homeostatic/neuroprotective morphological and cytokine profile, similar to that in an uninjured retina. This implies an hNGFp-mediated resolution of retinal inflammation, which prevents and/or rescues RGC death.

In line with these results, TrkA receptor is expressed only by ameboid Iba1+ cells in both unlesioned and lesioned neonatal retinae. This TrkA-positive microglia subpopulation represents a hallmark of a response to injury, leading to a large increase in the proportion of ramified microglia in the retinae treated with hNGFp, but not with hNGFwt. Above all, the TrkA-positive ameboid microglia subpopulation represents a lesion-promoted cellular target, receptive to hNGFp.

The regulatory mechanisms whereby the expression of TrkA is increased in ameboid microglia and is shut down upon returning to the ramified state remain to be ascertained. The Runx1 transcription factor, whose function is linked to TrkA lineage (Liu & Ma, 2011), might represent a key transcriptional mediator of the above mechanism. Indeed, Runx1 regulates the development of TrkA+ sensory neurons and bidirectionally controls TrkA expression (Liu & Ma, 2011; Marmigère et al., 2006). As for microglia in the mouse brain, Runx1 controls the activation state of microglia by inhibiting amoeboid microglia proliferation and promoting progression to the ramified state (Kierdorf & Prinz, 2013; Zusso et al., 2012). Interestingly, Runx1 expression is upregulated in brain microglia following nerve injury (Zusso et al., 2012). Thus, in the retina, the state-dependent expression of TrkA in microglia might be regulated by Runx1.

We conclude that the lesion enhances the appearance of a subpopulation of microglia cells, 'awaiting' to be pharmacologically targeted for a therapeutic neuroprotection. Hence, hNGFp targets a microglia cell population that is triggered as part of a homeostatic response to the lesion.

5 | CONCLUSION

In conclusion, results from this study indicate that a more effective TrkA-mediated neuroprotection by NGF-based drugs should not only involve activation of TrkA-mediated survival signals but also avoid additional concomitant stimulation of a death signal by p75NTR. hNGFp selectively activates the TrkA signalling stream without activating p75NTR, thus potentially re-establishing a signalling equilibrium.

All these properties displayed by hNGFp make it a master drug candidate for ocular indications. Actually, an eye drop hNGFp GMP formulation is being investigated in an ongoing clinical trial for the neuroprotection of RGC neurodegeneration to counteract visual loss in optic pathway glioma patients (NCT05733572). Moreover, our ongoing evaluation of effects of hNGFp treatment in a chronic glaucoma model could further reinforce the interest of hNGFp as a neuroprotective ocular therapy. This study lays the foundation for new vistas on microglia as central drivers of ocular pathology and visual loss. Molecules, such as hNGFp, promoting microglia homeostatic and neuroprotective function represent therefore a promising pharmacological approach to treat visual disease.

(equal). **Ivan Arisi:** Formal analysis (equal). **Rita Florio:** Methodology (equal). **Hiroki Asari:** Data curation (equal); formal analysis (equal). **Simona Capsoni:** Formal analysis (equal); investigation (equal). **Enrica Strettoi:** Methodology (equal). **Gino Villetti:** Project administration (equal). **Bruno Pietro Imbimbo:** Project administration (equal). **Massimo Dal Monte:** Project administration (supporting); supervision (supporting). **Romina Nassini:** Conceptualization (supporting); formal analysis (supporting); funding acquisition (supporting); resources (supporting); supervision (supporting). **Pierangelo Geppetti:** Funding acquisition (equal); project administration (equal); resources (equal). **Silvia Marinelli:** Conceptualization (lead); data curation (equal); formal analysis (equal); funding acquisition (equal); resources (equal); supervision (lead); validation (equal); visualization (lead); writing—original draft (lead); writing—review and editing (lead). **Antonino Cattaneo:** Conceptualization (lead); project administration (lead); resources (lead); writing—review and editing (supporting).

DATA AVAILABILITY STATEMENT

The data that support the findings of this study are available from the corresponding author upon reasonable request

DECLARATION OF TRANSPARENCY AND SCIENTIFIC RIGOUR

This declaration acknowledges that this paper adheres to the principles for transparent reporting and scientific rigour of preclinical research as stated in the BJP guidelines for Design and Analysis, Immunoblotting and Immunochemistry and Animal Experimentation and as recommended by funding agencies, publishers and other organizations engaged with supporting research.

ORCID

Massimo Dal Monte https://orcid.org/0000-0002-5181-4456
Romina Nassini https://orcid.org/0000-0002-9223-8395
Silvia Marinelli https://orcid.org/0000-0003-2620-8371

REFERENCES

Apfel, S. C., Schwartz, S., Adornato, B. T., Freeman, R., Biton, V., Rendell, M., Vinik, A., Giuliani, M., Stevens, J. C., Barbano, R., Dyck, P. J., & rhNGF Clinical Investigator Group. (2000). Efficacy and safety of recombinant human nerve growth factor in patients with diabetic polyneuropathy: A randomized controlled trial. rhNGF Clinical Investigator Group. *JAMA*, *284*, 2215–2221. https://doi.org/10.1001/jama.284.17.2215

Bai, Y., Dergham, P., Nedev, H., Xu, J., Galan, A., Rivera, J. C., ZhiHua, S., Mehta, H. M., Woo, S. B., Sarunic, M. V., Neet, K. E., & Saragovi, H. U. (2010). Chronic and acute models of retinal neurodegeneration TrkA activity are neuroprotective whereas p75NTR activity is neurotoxic through a paracrine mechanism. *The Journal of Biological Chemistry*, *285*, 39392–39400. https://doi.org/10.1074/jbc.M110.147801

Bellver-Landete, V., Bretheau, F., Mailhot, B., Vallières, N., Lessard, M., Janelle, M. E., Vernoux, N., Tremblay, M. È., Fuehrmann, T., Shoichet, M. S., & Lacroix, S. (2019). Microglia are an essential component of the neuroprotective scar that forms after spinal cord injury. *Nature Communications*, *10*, 518. https://doi.org/10.1038/s41467-019-08446-0

Benhar, I., Ding, J., Yan, W., Whitney, I. E., Jacobi, A., Sud, M., Burgin, G., Shekhar, K., Tran, N. M., Wang, C., He, Z., Sanes, J. R., & Regev, A. (2023). Temporal single-cell atlas of non-neuronal retinal cells reveals dynamic, coordinated multicellular responses to central nervous system injury. *Nature Immunology*, *24*, 700–713. https://doi.org/10.1038/s41590-023-01437-w

Blöchl, A., & Blöchl, R. (2007). A cell-biological model of p75NTR signaling: Cell-biological model of p75 signaling. *Journal of Neurochemistry*, *102*, 289–305. https://doi.org/10.1111/j.1471-4159.2007.04496.x

Bodeutsch, N., & Thanos, S. (2000). Migration of phagocytotic cells and development of the murine intraretinal microglial network: An in vivo study using fluorescent dyes. *Glia*, *32*, 91–101. https://doi.org/10.1002/1098-1136(200010)32:1<91::AID-GLIA90>3.0.CO;2-X

Bonini, S., Lambiase, A., Rama, P., Sinigaglia, F., Allegretti, M., Chao, W., Mantelli, F., Bonini, S., Lambiase, A., Rama, P., Messmer, E., Aragona, P., Geerling, G., Mastropasqua, L., Mencucci, R., Dart, J., Leonardi, A., Montero, J., Rolando, M., … Torrao, L. (2018). Phase II randomized, double-masked, vehicle-controlled trial of recombinant human nerve growth factor for neurotrophic keratitis. *Ophthalmology*, *125*, 1332–1343. https://doi.org/10.1016/j.ophtha.2018.02.022

Bruno, M. A., & Cuello, A. C. (2006). Activity-dependent release of precursor nerve growth factor, conversion to mature nerve growth factor, and its degradation by a protease cascade. *Proceedings of the National Academy of Sciences*, *103*, 6735–6740. https://doi.org/10.1073/pnas.0510645103

Capsoni, S. (2014). From genes to pain: Nerve growth factor and hereditary sensory and autonomic neuropathy type V. *The European Journal of Neuroscience*, *39*, 392–400. https://doi.org/10.1111/ejn.12461

Capsoni, S., & Cattaneo, A. (2022). Getting into the brain: The intranasal approach to enhance the delivery of nerve growth factor and its painless derivative in Alzheimer's disease and Down syndrome. *Frontiers in Neuroscience*, *16*, 773347. https://doi.org/10.3389/fnins.2022.773347

Capsoni, S., Covaceuszach, S., Marinelli, S., Ceci, M., Bernardo, A., Minghetti, L., Ugolini, G., Pavone, F., & Cattaneo, A. (2011). Taking pain out of NGF: A 'painless' NGF mutant, linked to hereditary sensory autonomic neuropathy type V, with full neurotrophic activity. *PLoS ONE*, *6*, e17321. https://doi.org/10.1371/journal.pone.0017321

Capsoni, S., Malerba, F., Carucci, N. M., Rizzi, C., Criscuolo, C., Origlia, N., Calvello, M., Viegi, A., Meli, G., & Cattaneo, A. (2017). The chemokine CXCL12 mediates the anti-amyloidogenic action of painless human nerve growth factor. *Brain: a Journal of Neurology*, *140*, 201–217. https://doi.org/10.1093/brain/aww271

Carmignoto, G., Comelli, M. C., Candeo, P., Cavicchioli, L., Yan, Q., Merighi, A., & Maffei, L. (1991). Expression of NGF receptor and NGF receptor mRNA in the developing and adult rat retina. *Experimental Neurology*, *111*, 302–311. https://doi.org/10.1016/0014-4886(91)90097-V

Cattaneo, A., Capsoni, S., Margotti, E., Righi, M., Kontsekova, E., Pavlik, P., Filipcik, P., & Novak, M. (1999). Functional blockade of tyrosine kinase A in the rat basal forebrain by a novel antagonistic anti-receptor

monoclonal antibody. *Journal of Neuroscience: the Official Journal of the Society for Neuroscience*, 19, 9687–9697. https://doi.org/10.1523/JNEUROSCI.19-22-09687.1999

Chao, M. V. (2003). Neurotrophins and their receptors: A convergence point for many signalling pathways. *Nature Reviews. Neuroscience*, 4, 299–309. https://doi.org/10.1038/nrn1078

Chen, M., & Xu, H. (2015). Parainflammation, chronic inflammation, and age-related macular degeneration. *Journal of Leukocyte Biology*, 98, 713–725. https://doi.org/10.1189/jlb.3RI0615-239R

Colafrancesco, V., Coassin, M., Rossi, S., & Aloe, L. (2011). Effect of eye NGF administration on two animal models of retinal ganglion cells degeneration. *Annali dell'Istituto Superiore di Sanità*, 47, 284–289. https://doi.org/10.4415/ANN_11_03_08

Conroy, J. N., & Coulson, E. J. (2022). High-affinity TrkA and p75 neurotrophin receptor complexes: A twisted affair. *The Journal of Biological Chemistry*, 298, 101568. https://doi.org/10.1016/j.jbc.2022.101568

Covaceuszach, S., Capsoni, S., Marinelli, S., Pavone, F., Ceci, M., Ugolini, G., Vignone, D., Amato, G., Paoletti, F., Lamba, D., & Cattaneo, A. (2010). In vitro receptor binding properties of a 'painless' NGF mutein, linked to hereditary sensory autonomic neuropathy type V. *Biochemical and Biophysical Research Communications*, 391, 824–829. https://doi.org/10.1016/j.bbrc.2009.11.146

CZI Single-Cell Biology Program. Abdulla, S., Aevermann, B., Assis, P., Badajoz, S., Bell, S. M., Bezzi, E., Cakir, B., Chaffer, J., Chambers, S., & Cherry, J. M. (2023). *CZ CELL×GENE Discover: A single-cell data platform for scalable exploration, analysis and modeling of aggregated data*. https://doi.org/10.1101/2023.10.30.563174.

Danneman, P. J., & Mandrell, T. D. (1997). Evaluation of five agents/-methods for anesthesia of neonatal rats. *Laboratory Animal Science*, 47(4), 386–395.

Davis, E. J., Foster, T. D., & Thomas, W. E. (1994). Cellular forms and functions of brain microglia. *Brain Research Bulletin*, 34, 73–78. https://doi.org/10.1016/0361-9230(94)90189-9

de Petrocellis, L., Guida, F., Moriello, A. S., de Chiaro, M., Piscitelli, F., de Novellis, V., Maione, S., & di Marzo, V. (2011). N-palmitoyl-vanillamide (palvanil) is a non-pungent analogue of capsaicin with stronger desensitizing capability against the TRPV1 receptor and anti-hyperalgesic activity. *Pharmacological Research*, 63, 294–299. https://doi.org/10.1016/j.phrs.2010.12.019

Dechant, G., & Barde, Y.-A. (2002). The neurotrophin receptor p75(NTR): Novel functions and implications for diseases of the nervous system. *Nature Neuroscience*, 5, 1131–1136. https://doi.org/10.1038/nn1102-1131

Einarsdottir, E., Carlsson, A., Minde, J., Toolanen, G., Svensson, O., Solders, G., Holmgren, G., Holmberg, D., & Holmberg, M. (2004). A mutation in the nerve growth factor beta gene (NGFB) causes loss of pain perception. *Human Molecular Genetics*, 13, 799–805. https://doi.org/10.1093/hmg/ddh096

Eriksdotter Jönhagen, M., Nordberg, A., Amberla, K., Bäckman, L., Ebendal, T., Meyerson, B., Olson, L., Seiger, Å., Shigeta, M., Theodorsson, E., Viitanen, M., Winblad, B., & Wahlund, L. O. (1998). Intracerebroventricular infusion of nerve growth factor in three patients with Alzheimer's disease. *Dementia and Geriatric Cognitive Disorders*, 9, 246–257. https://doi.org/10.1159/000017069

Falsini, B., Chiaretti, A., Rizzo, D., Piccardi, M., Ruggiero, A., Manni, L., Soligo, M., Dickmann, A., Federici, M., Salerni, A., Timelli, L., Guglielmi, G., Lazzareschi, I., Caldarelli, M., Galli-Resta, L., Colosimo, C., & Riccardi, R. (2016). Nerve growth factor improves visual loss in childhood optic gliomas: A randomized, double-blind, phase II clinical trial. *Brain: a Journal of Neurology*, 139, 404–414. https://doi.org/10.1093/brain/awv366

Frade, J. M., & Barde, Y. A. (1998). Microglia-derived nerve growth factor causes cell death in the developing retina. *Neuron*, 20, 35–41. https://doi.org/10.1016/S0896-6273(00)80432-8

Frade, J. M., Rodríguez-Tébar, A., & Barde, Y. A. (1996). Induction of cell death by endogenous nerve growth factor through its p75 receptor. *Nature*, 383, 166–168. https://doi.org/10.1038/383166a0

Galli-Resta, L., & Ensini, M. (1996). An intrinsic time limit between genesis and death of individual neurons in the developing retinal ganglion cell layer. *Journal of Neuroscience: the Official Journal of the Society for Neuroscience*, 16, 2318–2324. https://doi.org/10.1523/JNEUROSCI.16-07-02318.1996

Galvao, J., Elvas, F., Martins, T., Cordeiro, M. F., Ambrósio, A. F., & Santiago, A. R. (2015). Adenosine A3 receptor activation is neuroprotective against retinal neurodegeneration. *Experimental Eye Research*, 140, 65–74. https://doi.org/10.1016/j.exer.2015.08.009

Garcia, T. B., Hollborn, M., & Bringmann, A. (2017). Expression and signaling of NGF in the healthy and injured retina. *Cytokine & Growth Factor Reviews*, 34, 43–57. https://doi.org/10.1016/j.cytogfr.2016.11.005

Garcia-Valenzuela, E., Sharma, S. C., & Piña, A. L. (2005). Multilayered retinal microglial response to optic nerve transection in rats. *Molecular Vision*, 11, 225–231.

Guo, L., Davis, B. M., Ravindran, N., Galvao, J., Kapoor, N., Haamedi, N., Shamsher, E., Luong, V., Fico, E., & Cordeiro, M. F. (2020). Topical recombinant human nerve growth factor (rh-NGF) is neuroprotective to retinal ganglion cells by targeting secondary degeneration. *Scientific Reports*, 10, 3375. https://doi.org/10.1038/s41598-020-60427-2

Gupta, M. P., Herzlich, A. A., Sauer, T., & Chan, C.-C. (2016). Retinal anatomy and pathology. *Developments in Ophthalmology*, 55, 7–17. https://doi.org/10.1159/000431128

Gupta, N., Brown, K. E., & Milam, A. H. (2003). Activated microglia in human retinitis pigmentosa, late-onset retinal degeneration, and age-related macular degeneration. *Experimental Eye Research*, 76, 463–471. https://doi.org/10.1016/S0014-4835(02)00332-9

Gupta, N., Shyamasundar, S., Patnala, R., Karthikeyan, A., Arumugam, T. V., Ling, E. A., & Dheen, S. T. (2018). Recent progress in therapeutic strategies for microglia-mediated neuroinflammation in neuropathologies. *Expert Opinion on Therapeutic Targets*, 22, 765–781. https://doi.org/10.1080/14728222.2018.1515917

Hamrah, P., Yavuz Saricay, L., & Ozmen, M. C. (2022). Cutting edge: Topical recombinant nerve growth factor for the treatment of neurotrophic keratopathy-biologicals as a novel therapy for neurotrophic keratopathy. *Cornea*, 41, 673–679. https://doi.org/10.1097/ICO.0000000000002974

Holahan, M. R. (2017). A shift from a pivotal to supporting role for the growth-associated protein (GAP-43) in the coordination of axonal structural and functional plasticity. *Frontiers in Cellular Neuroscience*, 11, 266. https://doi.org/10.3389/fncel.2017.00266

Katz, L. C., & Shatz, C. J. (1996). Synaptic activity and the construction of cortical circuits. *Science*, 274, 1133–1138. https://doi.org/10.1126/science.274.5290.1133

Kierdorf, K., & Prinz, M. (2013). Factors regulating microglia activation. *Frontiers in Cellular Neuroscience*, 7, 44. https://doi.org/10.3389/fncel.2013.00044

Kumar, D., Li, H., Das, U. K., Syed, A. M., & El-Atab, N. (2023). Flexible solution-processable black-phosphorus-based optoelectronic memristive synapses for neuromorphic computing and artificial visual perception applications. *Advanced Materials*, 35, 2300446. https://doi.org/10.1002/adma.202300446

Lambiase, A., & Aloe, L. (1996). Nerve growth factor delays retinal degeneration in C3H mice. *Graefe's Archive for Clinical and Experimental Ophthalmology*, 234(Suppl 1), S96–S100. https://doi.org/10.1007/BF02343055

Lambiase, A., Aloe, L., Centofanti, M., Parisi, V., Mantelli, F., Colafrancesco, V., Manni, G. L., Bucci, M. G., Bonini, S., & Levi-Montalcini, R. (2009). Experimental and clinical evidence of neuroprotection by nerve growth factor eye drops: Implications for glaucoma.

Proceedings of the National Academy of Sciences of the United States of America, *11*, 13469–13474. https://doi.org/10.1073/pnas.0906678106

Lambiase, A., Centofanti, M., Micera, A., Manni, G. L., Mattei, E., de Gregorio, A., de Feo, G., Bucci, M. G., & Aloe, L. (1997). Nerve growth factor (NGF) reduces and NGF antibody exacerbates retinal damage induced in rabbit by experimental ocular hypertension. *Graefe's Archive for Clinical and Experimental Ophthalmology*, *235*, 780–785. https://doi.org/10.1007/BF02332863

LaVail, M. M., Unoki, K., Yasumura, D., Matthes, M. T., Yancopoulos, G. D., & Steinberg, R. H. (1992). Multiple growth factors, cytokines, and neurotrophins rescue photoreceptors from the damaging effects of constant light. *Proceedings of the National Academy of Sciences of the United States of America*, *89*, 11249–11253. https://doi.org/10.1073/pnas.89.23.11249

Lebrun-Julien, F., Morquette, B., Douillette, A., Saragovi, H. U., & Di Polo, A. (2009). Inhibition of p75(NTR) in glia potentiates TrkA-mediated survival of injured retinal ganglion cells. *Molecular and Cellular Neurosciences*, *40*, 410–420. https://doi.org/10.1016/j.mcn.2008.12.005

Lee, R., Kermani, P., Teng, K. K., & Hempstead, B. L. (2001). Regulation of cell survival by secreted proneurotrophins. *Science*, *294*, 1945–1948. https://doi.org/10.1126/science.1065057

Lewin, G. R., Ritter, A. M., & Mendell, L. M. (1993). Nerve growth factor-induced hyperalgesia in the neonatal and adult rat. *Journal of Neuroscience: the Official Journal of the Society for Neuroscience*, *13*, 2136–2148. https://doi.org/10.1523/JNEUROSCI.13-05-02136.1993

Li, Y., Yang, H., Gao, Y., & He, W. (2023). Ocular adverse events of cenegermin used in neurotrophic keratopathy: An analysis of the FDA adverse event reporting system database. *Expert Opinion on Drug Safety*, *1–7*, 385–391. https://doi.org/10.1080/14740338.2023.2251389

Lilley, E., Stanford, S. C., Kendall, D. E., Alexander, S. P. H., Cirino, G., Docherty, J. R., George, C. H., Insel, P. A., Izzo, A. A., Ji, Y., Panettieri, R. A., Sobey, C. G., Stefanska, B., Stephens, G., Teixeira, M., & Ahluwalia, A. (2020). ARRIVE 2.0 and the British Journal of Pharmacology: Updated guidance for 2020. *British Journal of Pharmacology*, *177*, 3611–3616. https://doi.org/10.1111/bph.15178

Lim, J.-H. A., Stafford, B. K., Nguyen, P. L., Lien, B. V., Wang, C., Zukor, K., He, Z., & Huberman, A. D. (2016). Neural activity promotes long-distance, target-specific regeneration of adult retinal axons. *Nature Neuroscience*, *19*, 1073–1084. https://doi.org/10.1038/nn.4340

Liu, Y., & Ma, Q. (2011). Generation of somatic sensory neuron diversity and implications on sensory coding. *Current Opinion in Neurobiology*, *21*, 52–60. https://doi.org/10.1016/j.conb.2010.09.003

Maffei, L., & Galli-Resta, L. (1990). Correlation in the discharges of neighboring rat retinal ganglion cells during prenatal life. *Proceedings of the National Academy of Sciences of the United States of America*, *87*, 2861–2864. https://doi.org/10.1073/pnas.87.7.2861

Malerba, F., Bruni Ercole, B., Florio, R., & Cattaneo, A. (2021). A quantitative bioassay to determine the inhibitory potency of NGF-TrkA antagonists. *SLAS DISCOVERY: Advancing the Science of Drug Discovery*, *26*, 823–830. https://doi.org/10.1177/24725552211000672

Malerba, F., Paoletti, F., Bruni Ercole, B., Materazzi, S., Nassini, R., Coppi, E., Patacchini, R., Capsoni, S., Lamba, D., & Cattaneo, A. (2015). Functional characterization of human ProNGF and NGF mutants: Identification of NGF P61SR100E as a 'painless' lead investigational candidate for therapeutic applications. *PLoS ONE*, *10*, e0136425. https://doi.org/10.1371/journal.pone.0136425

Margeta, M. A., Yin, Z., Madore, C., Pitts, K. M., Letcher, S. M., Tang, J., Jiang, S., Gauthier, C. D., Silveira, S. R., Schroeder, C. M., Lad, E. M., Proia, A. D., Tanzi, R. E., Holtzman, D. M., Krasemann, S., Chen, D. F., & Butovsky, O. (2022). Apolipoprotein E4 impairs the response of neurodegenerative retinal microglia and prevents neuronal loss in glaucoma. *Immunity*, *55*, 1627–1644.e7. https://doi.org/10.1016/j.immuni.2022.07.014

Marmigère, F., Montelius, A., Wegner, M., Groner, Y., Reichardt, L. F., & Ernfors, P. (2006). The Runx1/AML1 transcription factor selectively regulates development and survival of TrkA nociceptive sensory neurons. *Nature Neuroscience*, *9*, 180–187. https://doi.org/10.1038/nn1631

Marrone, M. C., Morabito, A., Giustizieri, M., Chiurchiù, V., Leuti, A., Mattioli, M., Marinelli, S., Riganti, L., Lombardi, M., Murana, E., Totaro, A., Piomelli, D., Ragozzino, D., Oddi, S., Maccarrone, M., Verderio, C., & Marinelli, S. (2017). TRPV1 channels are critical brain inflammation detectors and neuropathic pain biomarkers in mice. *Nature Communications*, *8*, 15292. https://doi.org/10.1038/ncomms15292

Mey, J., & Thanos, S. (1993). Intravitreal injections of neurotrophic factors support the survival of axotomized retinal ganglion cells in adult rats in vivo. *Brain Research*, *602*, 304–317. https://doi.org/10.1016/0006-8993(93)90695-J

Pan, L., Cho, K. S., Wei, X., Xu, F., Lennikov, A., Hu, G., Tang, J., Guo, S., Chen, J., Kriukov, E., Kyle, R., Elzaridi, F., Jiang, S., Dromel, P. A., Young, M., Baranov, P., do, C. W., Williams, R. W., Chen, J., … Chen, D. F. (2023). IGFBPL1 is a master driver of microglia homeostasis and resolution of neuroinflammation in glaucoma and brain tauopathy. *Cell Reports*, *42*, 112889. https://doi.org/10.1016/j.celrep.2023.112889

Percie du Sert, N., Hurst, V., Ahluwalia, A., Alam, S., Avey, M. T., Baker, M., Browne, W. J., Clark, A., Cuthill, I. C., Dirnagl, U., Emerson, M., Garner, P., Holgate, S. T., Howells, D. W., Karp, N. A., Lazic, S. E., Lidster, K., MacCallum, C. J., Macleod,,M., … Würbel,,H. (2020). The ARRIVE guidelines 2.0: Updated guidelines for reporting animal research. *PLoS Biology*, *18*(7), e3000410. https://doi.org/10.1371/journal.pbio.3000410

Pezet, S., & McMahon, S. B. (2006). Neurotrophins: Mediators and modulators of pain. *Annual Review of Neuroscience*, *29*, 507–538. https://doi.org/10.1146/annurev.neuro.29.051605.112929

Pflugfelder, S. C., Massaro-Giordano, M., Perez, V. L., Hamrah, P., Deng, S. X., Espandar, L., Foster, C. S., Affeldt, J., Seedor, J. A., Afshari, N. A., Chao, W., Allegretti, M., Mantelli, F., & Dana, R. (2020). Topical recombinant human nerve growth factor (cenegermin) for neurotrophic keratopathy: A multicenter randomized vehicle-controlled pivotal trial. *Ophthalmology*, *127*, 14–26. https://doi.org/10.1016/j.ophtha.2019.08.020

Rabacchi, S. A., Ensini, M., Bonfanti, L., Gravina, A., & Maffei, L. (1994). Nerve growth factor reduces apoptosis of axotomized retinal ganglion cells in the neonatal rat. *Neuroscience*, *63*(4), 969–973. https://doi.org/10.1016/0306-4522(94)90565-7

Rathnasamy, G., Foulds, W. S., Ling, E.-A., & Kaur, C. (2019). Retinal microglia—A key player in healthy and diseased retina. *Progress in Neurobiology*, *173*, 18–40. https://doi.org/10.1016/j.pneurobio.2018.05.006

Rattenholl, A., Ruoppolo, M., Flagiello, A., Monti, M., Vinci, F., Marino, G., Lilie, H., Schwarz, E., & Rudolph, R. (2001). Pro-sequence assisted folding and disulfide bond formation of human nerve growth factor. *Journal of Molecular Biology*, *305*, 523–533. https://doi.org/10.1006/jmbi.2000.4295

Rizzi, C., Tiberi, A., Giustizieri, M., Marrone, M. C., Gobbo, F., Carucci, N. M., Meli, G., Arisi, I., D'Onofrio, M., Marinelli, S., Capsoni, S., & Cattaneo, A. (2018). NGF steers microglia toward a neuroprotective phenotype. *Glia*, *66*, 1395–1416. https://doi.org/10.1002/glia.23312

Sacchetti, M., Lambiase, A., Schmidl, D., Schmetterer, L., Ferrari, M., Mantelli, F., Allegretti, M., & Garhoefer, G. (2020). Effect of recombinant human nerve growth factor eye drops in patients with dry eye: A phase IIa, open label, multiple-dose study. *The British Journal of Ophthalmology*, *104*, 127–135. https://doi.org/10.1136/bjophthalmol-2018-312470

Savage, J. C., Carrier, M., & Tremblay, M.-È. (2019). Morphology of microglia across contexts of health and disease. *Methods in Molecular Biology*, *2034*, 13–26. https://doi.org/10.1007/978-1-4939-9658-2_2

Schafer, D. P., Lehrman, E. K., Kautzman, A. G., Koyama, R., Mardinly, A. R., Yamasaki, R., Ransohoff, R. M., Greenberg, M. E., Barres, B. A., & Stevens, B. (2012). Microglia sculpt postnatal neural circuits in an activity and complement-dependent manner. *Neuron*, *74*, 691–705. https://doi.org/10.1016/j.neuron.2012.03.026

Schoups, A. A., Elliott, R. C., Friedman, W. J., & Black, I. B. (1995). NGF and BDNF are differentially modulated by visual experience in the developing geniculocortical pathway. *Brain Research. Developmental Brain Research*, *86*, 326–334. https://doi.org/10.1016/0165-3806(95)00043-D

Shi, Z., Birman, E., & Saragovi, H. U. (2007). Neurotrophic rationale in glaucoma: A TrkA agonist, but not NGF or a p75 antagonist, protects retinal ganglion cells in vivo. *Developmental Neurobiology*, *67*, 884–894. https://doi.org/10.1002/dneu.20360

Siliprandi, R., Canella, R., & Carmignoto, G. (1993). Nerve growth factor promotes functional recovery of retinal ganglion cells after ischemia. *Investigative Ophthalmology & Visual Science*, *34*, 3232–3245.

Silverman, S. M., & Wong, W. T. (2018). Microglia in the retina: Roles in development, maturity, and disease. *Annu. Rev. vis. Sci.*, *4*, 45–77. https://doi.org/10.1146/annurev-vision-091517-034425

Smeyne, R. J., Klein, R., Schnapp, A., Long, L. K., Bryant, S., Lewin, A., Lira, S. A., & Barbacid, M. (1994). Severe sensory and sympathetic neuropathies in mice carrying a disrupted Trk/NGF receptor gene. *Nature*, *368*, 246–249. https://doi.org/10.1038/368246a0

Testa, G., Mainardi, M., Vannini, E., Pancrazi, L., Cattaneo, A., & Costa, M. (2022). Disentangling the signaling complexity of nerve growth factor receptors by CRISPR/Cas9. *The FASEB Journal*, *36*, e22498. https://doi.org/10.1096/fj.202101760RR

Thanos, S., Mey, J., & Wild, M. (1993). Treatment of the adult retina with microglia-suppressing factors retards axotomy-induced neuronal degradation and enhances axonal regeneration in vivo and in vitro. *The Journal of Neuroscience*, *13*, 455–466. https://doi.org/10.1523/JNEUROSCI.13-02-00455.1993

Tiberi, A., Borgonovo, G., Testa, G., Pacifico, P., Jacob, A., di Caprio, M., Totaro, V., Calvello, M., Cattaneo, A., & Capsoni, S. (2023). Reversal of neurological deficits by painless nerve growth factor in a mouse model of Rett syndrome. *Brain*, *147*(1), 122–134. https://doi.org/10.1093/brain/awad282

Tran, N. M., Shekhar, K., Whitney, I. E., Jacobi, A., Benhar, I., Hong, G., Yan, W., Adiconis, X., Arnold, M. K. E., Lee, J. M., Levin, J. Z., Lin, D., Wang, C., Lieber, C. M., Regev, A., He, Z., & Sanes, J. R. (2019). Single-cell profiles of retinal ganglion cells differing in resilience to injury reveal neuroprotective genes. *Neuron, 104*, 1039–1055.e12. https://doi.org/10.1016/j.neuron.2019.11.006

Varadarajan, S. G., Wang, F., Dhande, O. S., le, P., Duan, X., & Huberman, A. D. (2023). Postsynaptic neuronal activity promotes regeneration of retinal axons. *Cell Reports*, *42*, 112476. https://doi.org/10.1016/j.celrep.2023.112476

Villegas-Pérez, M. P., Vidal-Sanz, M., Rasminsky, M., Bray, G. M., & Aguayo, A. J. (1993). Rapid and protracted phases of retinal ganglion cell loss follow axotomy in the optic nerve of adult rats. *Journal of Neurobiology*, *24*, 23–36. https://doi.org/10.1002/neu.480240103

von Bartheld, C. S. (1998). Neurotrophins in the developing and regenerating visual system. *Histology and Histopathology*, *13*, 437–459.

Winn, B. J., Shin, E., Odel, J. G., Greenstein, V. C., & Hood, D. C. (2005). Interpreting the multifocal visual evoked potential: The effects of refractive errors, cataracts, and fixation errors. *The British Journal of Ophthalmology*, *89*, 340–344. https://doi.org/10.1136/bjo.2004.047910

Yger, P., Spampinato, G. L. B., Esposito, E., Lefebvre, B., Deny, S., Gardella, C., Stimberg, M., Jetter, F., Zeck, G., Picaud, S., Duebel, J., & Marre, O. (2018). A spike sorting toolbox for up to thousands of electrodes validated with ground truth recordings in vitro and in vivo. *eLife*, *7*, 1–23. https://doi.org/10.7554/eLife.34518

Yoon, S. O., Casaccia-Bonnefil, P., Carter, B., & Chao, M. V. (1998). Competitive signaling between TrkA and p75 nerve growth factor receptors determines cell survival. *Journal of Neuroscience: the Official Journal of the Society for Neuroscience*, *18*, 3273–3281. https://doi.org/10.1523/JNEUROSCI.18-09-03273.1998

Zanellato, A., Comelli, M. C., Dal Toso, R., & Carmignoto, G. (1993). Developing rat retinal ganglion cells express the functional NGF receptor p140trkA. *Developmental Biology*, *159*, 105–113. https://doi.org/10.1006/dbio.1993.1224

Zhao, L., Zabel, M. K., Wang, X., Ma, W., Shah, P., Fariss, R. N., Qian, H., Parkhurst, C. N., Gan, W. B., & Wong, W. T. (2015). Microglial phagocytosis of living photoreceptors contributes to inherited retinal degeneration. *EMBO Molecular Medicine*, *7*, 1179–1197. https://doi.org/10.15252/emmm.201505298

Zusso, M., Methot, L., Lo, R., Greenhalgh, A. D., David, S., & Stifani, S. (2012). Regulation of postnatal forebrain amoeboid microglial cell proliferation and development by the transcription factor Runx1. *Journal of Neuroscience: the Official Journal of the Society for Neuroscience*, *32*, 11285–11298. https://doi.org/10.1523/JNEUROSCI.6182-11.2012

SUPPORTING INFORMATION

Additional supporting information can be found online in the Supporting Information section at the end of this article.